

# The trace element composition of apatite and its application to detrital provenance studies



Gary O'Sullivan<sup>a,d,\*</sup>, David Chew<sup>a</sup>, Gavin Kenny<sup>b</sup>, Isadora Henrichs<sup>a</sup>, Dónal Mulligan<sup>c</sup>

<sup>a</sup> Department of Geology, Trinity College Dublin, The University of Dublin, Dublin 2, Ireland

<sup>b</sup> Department of Geosciences, Swedish Museum of Natural History, SE-104 05 Stockholm, Sweden

<sup>c</sup> School of Communications, Dublin City University, Dublin 9, Ireland

<sup>d</sup> School of Earth Sciences, University College Dublin, Dublin 4, Ireland

## ABSTRACT

Apatite's ubiquity in crystalline rocks, variable trace element contents (particularly with regard to the REE, actinides and Sr), and amenability to various dating techniques based on the decay of the radioisotopes U and Th, permit specific provenance determinations. In this study, we first present a comprehensive description of the trace element behaviour of apatite in various kinds of bedrocks (igneous rocks from felsic through to ultramafic compositions, metamorphic rocks from low to high grades and of diverse protolith composition, and authigenic apatite) in which we explain why apatite is so highly diverse in terms of its trace element composition. Next, we present a synthesis of bedrock apatite trace-element compositional data from previous work, assembling a library of apatite compositions that includes the most abundant apatite-bearing lithologies in the Earth's crust, and many other less abundant rock types. Compositional statistics, classification, and a machine learning classifier are then applied to this dataset to generate biplots that can be used to determine the broad source lithology of detrital apatite, with misclassification averaging 15%. This methodology is tested in three case studies to demonstrate its utility. In these examples, detrital apatite can be convincingly linked to different lithology types, and combined apatite trace-element and U–Pb data can determine the terranes from which individual apatites were likely derived. The addition of apatite trace-element information therefore enables the determination of the source lithology, making the extraction of novel information and more specific provenance determinations possible, and opening up new avenues in source-to-sink modelling.

## 1. Introduction

We here present the various defining geochemical characteristics of apatite from different rocks and crystallization environments, the applicability of geo- and thermo-chronology to apatite, and the behaviour of apatite in sedimentary systems. This is largely based on a synthesis of existing literature and is intended to introduce the geochemical and physical attributes of apatite that we consider to be most applicable to sedimentary provenance, tephra analysis, and ore-deposit vectoring; and discusses previous work using apatite compositions in these areas. This literature synthesis illustrates the rationale for our subsequent methodology, involving the compilation and treatment of apatite trace element compositional data that we have collated from the literature, and the subsequent application of compositional statistics to those data, chiefly using Principal Component Analysis (PCA) and a machine learning method Support Vector Machine (SVM). This introduction also aims to act as a useful synopsis of the current understanding of apatite trace element compositions in various lithologies, that currently exists in disparate literature. By doing so, it is our hope that this review can help the reader to appreciate the choice of element ratios later employed on biplots. Thereafter, the methodology we have developed for

trace element compositional analysis of apatite is applied to three previously published provenance case studies to demonstrate its utility, though the range of possible applications is substantially broader than sedimentary provenance alone.

### 1.1. Introduction to apatite

Apatite,  $\text{Ca}_5(\text{PO}_4)_3(\text{OH}, \text{F}, \text{Cl})$ , is a very common mineral group in the various lithologies that comprise the Earth's lithosphere (Chang et al., 1998). This is primarily due to the inability of the major rock-forming minerals to accommodate significant amounts of phosphorous within their crystal lattice (Piccoli and Candela, 2002). Apatite is also by far the most abundant phosphate mineral; monazite ( $[\text{La}, \text{Ce}, \text{Th}] \text{PO}_4$ ) and xenotime ( $\text{YPO}_4$ ) are the only other phosphate minerals in non-trivial abundance. The apatite mineral group has three natural end-member compositions, F-endmember fluorapatite, Cl-endmember chlorapatite and OH-group endmember hydroxyapatite, comprising a solid solution series; fluorapatite is by-far the most abundant apatite-group mineral in rocks (Chang et al., 1998).

Apatite is present in most igneous and metamorphic rocks and derived clastic sediments thereof (Piccoli and Candela, 2002), as

\* Corresponding author.

E-mail address: [gary.osullivan@ucd.ie](mailto:gary.osullivan@ucd.ie) (G. O'Sullivan).

sedimentary overgrowths (Bouch et al., 2002), and as biologically precipitated apatite, particularly in the mineralised body parts of vertebrates (e.g. Dorozkhin and Epple, 2002). Apatite is present as a rock-forming mineral only in certain igneous rocks such as pegmatites, cumulates such as nelsonites (e.g. Ihlen et al., 2014), and carbonatites; in phosphorites (the major global ore source of P for fertilisers) as carbonate-rich apatite (McArthur, 1985), and lastly in certain sedimentary rocks it is the cementing phase (e.g. Bouch et al., 2002). The name apatite, from the Greek ἀπάτη, means to deceive, owing to the diverse optical appearance of natural apatite (Roycroft and Cuypers, 2015), which in turn is a consequence of trace element substitutions in the apatite crystal lattice (e.g. Li et al., 1993). Amongst the most common substituting elements are the rare earth elements (REEs) and yttrium (REYs), Mn and Sr and the actinides U and Th, all of which substitute for Ca (note that some of these are coupled substitutions); the halogens F, Cl, Br and I (and OH) (Kusebauch et al., 2015); and small, highly charged ions that substitute for P such as Si, S, Na, As and V (Belousova et al., 2002a,b; Chang et al., 1998). Differences in the abundances of these elements are usually host-rock specific and can be used to trace the chemical environment in which individual apatite grains formed (Abdullin et al., 2016; Morton and Yaxley, 2007). Also, the incorporation of U and Th into the apatite lattice enables the routine dating of individual apatite grains by the fission track (e.g. Malusà and Fitzgerald, 2019) and (U–Th)/He methods (e.g. Ehlers and Farley, 2003), and the U–Pb method once a common-Pb correction has been applied (Chew and Donelick, 2012).

Due to the wide spectrum of elements incorporated into its lattice, apatite is being increasingly used as a geological tracer. Tracing applications include palaeodrainage and palaeotectonic reconstructions in basin analysis (e.g. Carrapa et al., 2009; Mark et al., 2016; Morton and Yaxley, 2007; Resentini and Malusà, 2012; Zattin et al., 2012), the correlation and chronology study of tephra layers (e.g. Sell et al., 2015) and the vectoring of ore-deposits (e.g. Belousova et al., 2002a,b; Glorie et al., 2019; Mao et al., 2016), including REE-placer deposits (e.g. Goodenough et al., 2016 and references therein). Additionally, the halogen and noble gas geochemistry of apatite is being increasingly used to study lunar formation (e.g. Boyce et al., 2014; McCubbin et al., 2011) and magma geochemistry and mantle geochemistry (Belousova et al., 2001; Matsumoto et al., 1997; O'Reilly and Griffin, 2000). As a detrital tracer, apatite is able to record both the age (e.g. Carrapa et al., 2009) and lithology of its source (e.g. Abdullin et al., 2016); by combining age and lithological information in detrital apatite it is therefore possible to make highly specific provenance determinations (e.g. Danišík, 2019; O'Sullivan et al., 2018).

## 2. Physical wear and chemical weathering properties of apatite

Amongst the non-opaque heavy mineral species apatite is less chemically stable on the Earth surface than some other detrital heavy minerals, particularly the ZTR (zircon, tourmaline, and rutile) assemblage (Hubert, 1962) “ultra-resistant” heavy minerals. This is because apatite is prone to dissolution by acidic meteoric waters (e.g. Morton and Hallsworth, 1999 and references therein). However, once buried in a sedimentary sequence apatite is often remarkably persistent during diagenesis, even often acquiring overgrowths due to the liberation of organic and adsorbed P (Bouch et al., 2002), and can sometimes even be the main cementing phase in detrital rocks (Joosu et al., 2016).

Physical wear is often incorrectly identified as an important cause for the breakdown and ultimate destruction of mineral phases in detritus, the so-called “maturity myth” described by Garzanti (2017). Instead, detrital assemblages (with the exception of unconsolidated or soluble rock fragments and minerals, e.g. Picard et al., 2007) typically do not evolve at a meaningful rate to more “mature” assemblages with increasing transport distance or time. This has been demonstrated many times in natural settings (e.g. Garzanti et al., 2018; Picard et al., 2007; Russell, 1937) and also in controlled laboratory settings (Kuenen, 1960;

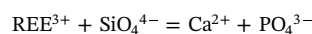
Kuenen, 1956; Kuenen, 1959); the existence of placer deposits of very soft minerals such as monazite also support these findings (e.g. Dill et al., 2012). Therefore, by discounting abrasion as a means of destroying mineral species in typical clastic sediments (with the exception of aeolian settings, Garzanti, 2017), the presence or absence of apatite in a given sediment can mostly be attributed to two factors. These are: 1) the abundance (or fertility) of apatite in the source material (e.g. Malusà et al., 2016), which will only be very low if the source rocks are phosphorous-poor (such as most chemically-precipitated sediments apart from phosphorites, or depleted mantle rocks), or high-P K-feldspar bearing (e.g. London, 1992), and 2) the degree to which acidic chemical weathering has altered the detrital assemblage - whether in transport-limited (i.e. soil/humus forming) settings at the apatite source, during prolonged alluvial storage such as humid flood plain environments, or if the early diagenetic fluids are particularly acidic (Morton and Hallsworth, 1999 and references therein).

Apatite is hence often abundant in sediments, with abundances of 20–40% apatite not uncommon in modern fluvial heavy mineral assemblages (e.g. Bernoulli and Winkler, 1990; O'Sullivan et al., 2018), while apatite is almost never absent in Quaternary sedimentary deposits worldwide (e.g. Nechaev and Ispording, 1993). Large volumes of detrital apatite in very old sediments can survive to the present day, themselves preserving apatite billions of years old (e.g. Kenny et al., 2019). Indeed, Archaean apatite U–Pb ages are obtained from cratonic basement (and are even sometimes *better-preserved* than zircon U–Pb ages for the same rocks due to Pb-loss in co-genetic zircon, e.g. Oosthuizen and Burger, 1973), as many cratons have experienced negligible deformation since their stabilization (King, 2005).

### 2.1. Geochemistry of apatite

In order to use apatite as a tracer, it is crucial that its trace-element chemistry in all of the diverse environments that apatite can occur (magmatic systems, low-grade metamorphic systems, diagenetic environments etc.) is well characterised. This section thus provides a framework to explain why apatite from different bedrock lithologies is so readily separated on a PCA biplot, and to understand the nature and geometry of that separation, as shown in section 3. Igneous apatite is considered first, followed by low-grade metamorphic apatite; refractory apatite in metamorphic rocks; metasomatic apatite; high-grade metamorphic apatite; and finally, authigenic apatite.

The apatite unit cell can be simplified to the formula  $A_5(XO_4)_3Z$  and typically exhibits a hexagonal crystallographic structure. The A-site hosts Ca in two structural sites, the IX-fold coordinated Ca1 site, and the VII-fold coordinated Ca2 site. The IV-fold X site hosts  $P^{5+}$ , and lastly, the monovalent Z-site hosts a halogen (Cl or F, with trace quantities of Br and I), an  $OH^-$  group, or a vacancy. Substituting elements in the A-site may include significant quantities of  $Sr^{2+}$ ,  $Mn^{2+}$ ,  $Pb^{2+}$ ,  $U^{4+}$  and  $Th^{4+}$ . In the X-site,  $PO_4^{3-}$  can be replaced by small, highly charged cations such as  $S^{6+}$ ,  $As^{5+}$ ,  $V^{5+}$ , and  $Si^{4+}$ . Triply-charged REYs $^{3+}$  (REY = REE + Y) substitute into apatite via coupled substitution processes, with the main substitution mechanisms in geological systems being (e.g. Ronsbo, 1989):



REYs and Sr strongly partition into apatite in igneous melts, thus in magmatic systems apatite can control a significant portion of the whole-rock REE- and Sr-budget, and can be a useful tracer in igneous petrogenesis studies (Prowatke and Klemme, 2006). While some high-field-strength elements (HFSEs) such as U and Th are compatible in apatite (to the extent that apatite can control the whole-rock U- and Th-budgets in lithologies where other actinide-hosts are absent (e.g. O'Reilly and Griffin, 2000), most other HFSEs (e.g. Zr, Hf, Nb, Ta, Ti etc.) and the large-ion lithophile elements (LILEs; particularly the very largest such

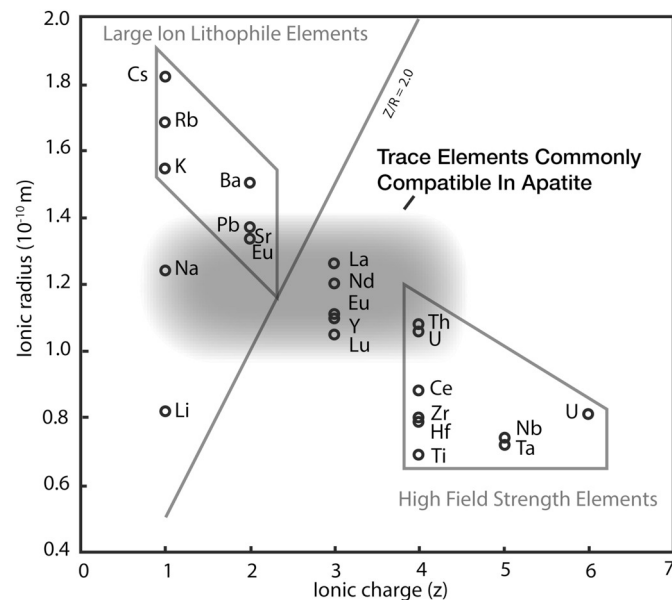


**Fig. 1.** Plot of ionic radius versus ionic charge modified from Whittaker and Muntus (1970). The most commonly compatible elements in apatite are approximately delimited by the shaded area and exhibit ionic radii between  $0.9$  and  $1.4 \cdot 10^{-10} \text{ m}$ . Elements such as Ba and Li may sometimes be incorporated in apatite under certain special conditions (e.g. authigenic apatite/francolite precipitated from seawater).

as Rb, Cs etc.) are not preferentially partitioned into apatite in igneous and metamorphic rocks (Fig. 1).

### 2.1.1. Igneous apatite geochemistry

In magmatic rocks apatite is a minor yet ubiquitous accessory phase. Apatite is occasionally a rock forming mineral in some cumulates and rare igneous rock types such as nelsonites and certain pegmatites (Piccoli and Candela, 2002), while it may be absent in some S-type granitoids in which the high solubility of apatite means that P-bearing K-feldspar instead incorporates the whole-rock P-budget (e.g. London, 1992). Apatite from igneous rocks is typically more actinide-rich and common-Pb ( $\text{Pb}_{\text{C}}$ ) depleted than metamorphic apatite, and thus often plots closer to concordia, providing more precise U–Pb ages (e.g. O'Sullivan et al., 2018; Henrichs et al., 2018). Igneous apatite thus will be overrepresented compared to metamorphic apatite in detrital apatite datasets acquired using only U–Pb dating techniques. This is because apatite in pelites is typically low-U detrital metamorphic grains will yield larger associated single grain U–Pb age uncertainties, and due to the common-Pb corrections necessary to undertake most apatite U–Pb dating U–Pb data quality is often monitored using precision cut-offs rather than by measuring discordance (e.g. Mark et al., 2016; O'Sullivan et al., 2016, 2018). The dominant factors controlling apatite solubility and crystallization in igneous rocks are  $\text{SiO}_2$  and  $\text{P}_2\text{O}_5$  concentrations in the melt, and melt temperature. Apatite solubility is thus strongly correlated to the degree of crustal contamination in the melt, with apatite in anatexitic melts having much greater solubility than apatite in mafic igneous rocks (Hsieh et al., 2008). Water content, pressure and the concentration of Ca in the melt are not important factors governing apatite solubility (Piccoli and Candela, 2002 and references therein).

Igneous apatite has been used successfully as a petrogenetic tool in many studies. Sha and Chappell (1999) demonstrated that apatite from crustal contaminated “S-type” granites and felsic “I-type” granites is depleted in the light rare earth elements (LREEs) and Th, whereas apatite from more juvenile I-type granites (“mafic granites”) generally contains similar (or even enriched) chondrite-normalised abundances of these elements compared to the middle rare earths (MREEs) and U respectively.

Following from the findings of Sha and Chappell (1999) regarding REE-patterns in granitoid apatite, authors such as Belousova et al. (2001) and Hsieh et al. (2008) proposed that the difference in trace element contents of apatite from felsic vs mafic granites (i.e. juvenile, less contaminated granites) is largely determined by the aluminium saturation index (ASI) of the magma rather than its  $\text{SiO}_2$  content or the degree of fractionation of the host melt. As monazite crystallises as a primary phase in high ASI (i.e.  $\text{ASI} > 1.1$ ) rocks, the typical shape of chondrite-normalised apatite REE-plots in felsic melts (e.g. the LREE depletion in S-type granitoid apatite [S] relative to other igneous lithologies; Fig. Error! Reference source not found.) may therefore be explained by the coeval or later crystallization of apatite with respect to monazite, which reduces the amounts of Th and LREE available to apatite. Consequently, La/Sm ratios may thus be used to recognise such magmas as there is strong partitioning between La and Sm in monazite, and this fingerprint may be recorded in cogenetic apatite. However, as apatite solubility is strongly correlated to the degree of crustal contamination in the melt (Piccoli and Candela, 2002), it is feasible that the REE-composition of igneous apatite may also be related to the timing of crystallization of apatite relative to feldspar (which incorporates significant Sr, La, Ce, Pr and Eu, e.g. Larsen, 2002). As apatite is late crystallising in felsic rocks (La- and Ce-poor, large Eu-anomalies, very low Sr-contents – S-type granitoid apatite [S], Fig. 2) may be explained by the late crystallization of apatite relative to rock-forming feldspar. P-incorporation by K-feldspar in very felsic melts with very high apatite solubility can also prevent the crystallization of apatite entirely (London, 1992).

Biplots of Sr vs Mn in apatite are also useful to constrain the host-magma composition and to determine both the degree of magma fractionation and the oxygen fugacity of the melt (e.g. Sha and Chappell, 1999; Hsieh et al., 2008). The apatite Sr/Mn ratio is usually i) very low in apatite from highly fractionated melts due to the elevated apatite Mn-contents in such systems (up to 1 wt% or more), ii) close to unity (1:1) in I-type granitoids (abundances of tens or several hundred ppm for each element), and iii) very high in mafic melts (due to elevated Sr-contents of up to several thousand ppm) (Belousova et al., 2001; Tang et al., 2012). Features common to nearly allapatites from granitoids include pronounced negative Eu-anomalies (primarily due to crystallization after feldspar, and whole rock REE chemistry), and generally high  $\Sigma\text{REE}$  abundances.

Apatite in mafic igneous rocks [IM] systematically differs from apatite in felsic granitoids [S] in its trace-element composition (Fig. 2). The La/Lu ratios are higher as a result of the melt composition of the mafic source and also the absence of cogenetic monazite crystallization (e.g. Belousova et al., 2002a,b), resulting in strongly LREE-enriched REE-profiles. Th/U and Sr/Mn ratios are also typically higher than in granitoid apatite, while Eu-anomalies vary depending on whether apatite crystallises before or after feldspar (e.g. Tang et al., 2012), and may even be mildly positive in feldspar-absent rocks such as lherzolites or carbonatites ([UM] Fig. 2, e.g. O'Reilly and Griffin, 2000). Apatite from those ultramafic lithologies may also be readily discriminated from mafic apatite as ultramafic apatite is much more enriched in Sr, and extremely depleted in the HREEs (O'Reilly and Griffin, 2000; Tang et al., 2012).

Lastly, apatite from alkali-rich igneous rocks typically has very elevated REE contents (Syenite and Phonolite [ALK] panel on Fig. 2). In particular, LREE contents are usually extremely enriched, with wt% contents of LREEs reported in studies of apatite from syenitic, agpaitic and phonolitic rocks (e.g. Ronso, 1989; Zirner et al., 2015). This REE behaviour of apatite from alkali-rich igneous rocks permits its discrimination from other igneous apatite.

### 2.1.2. Low- and medium-grade metamorphic apatite geochemistry

The abundances and elemental ratios of trace elements of neocrystalline and reprecipitated apatite in low- and medium-grade

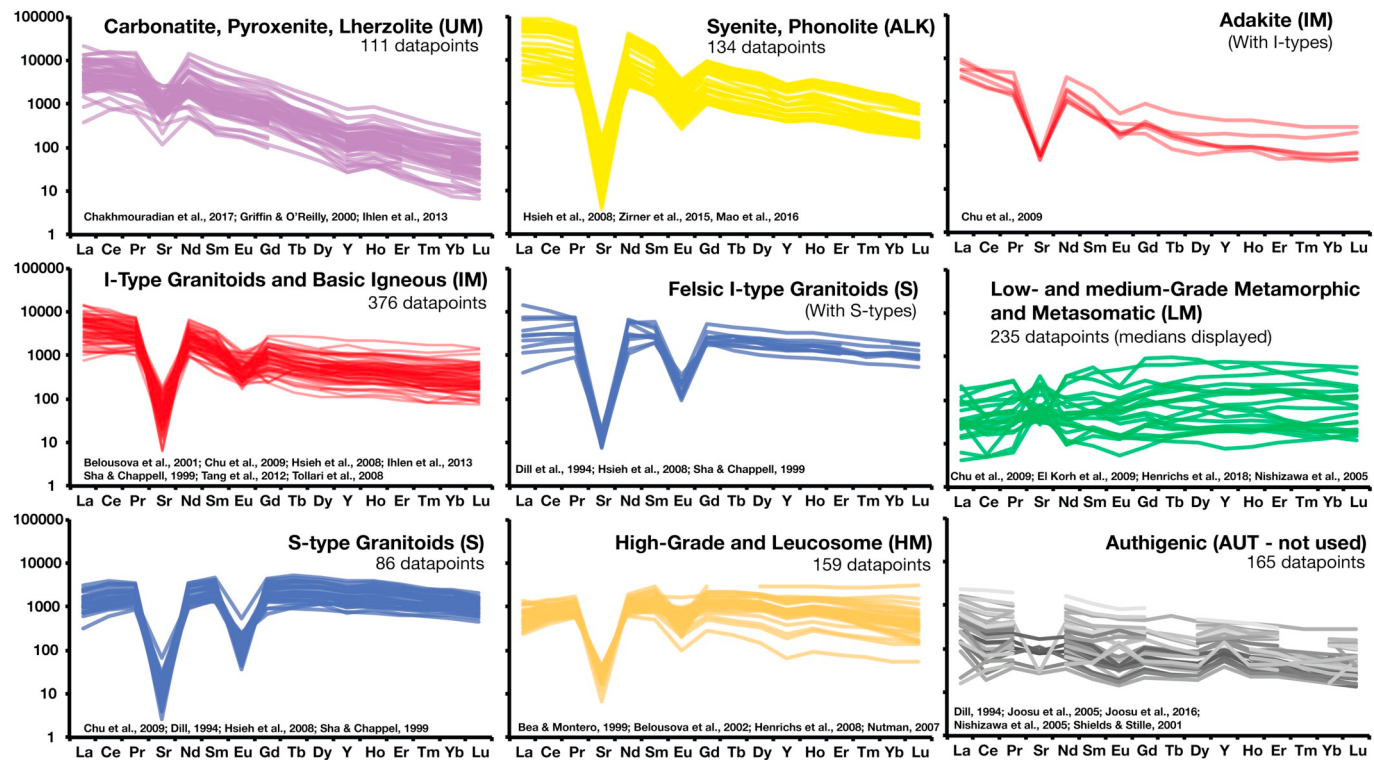


**Fig. 2.** Chondrite-normalised (McDonough and Sun, 1995) REY + Sr multi-element plots ('spidergrams') of apatite from different categories of igneous rocks, low- and high-grade metamorphic apatite, and authigenic and fossil apatite (~ 350 rocks samples from the literature). All data were acquired by LA-ICPMS (supplementary file S1). Gaps on the graphs represent non-analysed elements. The authors of the respective studies classified the host lithologies. In some diagrams presented later in this study, some groups were amalgamated and are thus given the same codes and colouring. The same data suite, classifications and abbreviations (in brackets beside the descriptions) are used throughout this article. Note that authigenic apatite is not used on subsequent plots due to the high proportion of data-points with missing elements.

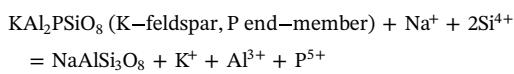
metamorphic rocks (i.e. super-anchizone to sub-anatectic conditions) are highly distinct compared to those of magmatic apatite. Apatite in these rocks often have very variable and complex chondrite-normalised REE spectra (e.g. Henrichs et al., 2019), but with typically extremely low ΣREE abundances ("LM" panel on Fig. 2). Eu-anomalies vary from mildly negative to positive with typically low actinide contents, especially Th (e.g. Bea and Montero, 1999; El Khor et al., 2009; Henrichs et al., 2018, 2019; Nutman, 2007). Low- to medium-grade metamorphic rocks rarely preserve equilibrium assemblages even on a thin-section scale, as the reaction rates are slow compared with rates of change in the physical conditions the rock has experienced (P, T or changes in fluid composition) (e.g. Lanari et al., 2017). Low reaction rates result in incomplete reactions and chemical disequilibrium, and apatite grains from the same low-grade metamorphic rock samples can exhibit orders of magnitude variation in trace-element abundances (e.g. Gaweda et al., 2018).

Though the trace element signature of low- to medium-grade metamorphic apatite is highly distinct to that of igneous apatite, definitive discrimination of metamorphic apatite from different protolith types is not yet possible, with apatite from mafic and pelitic lithologies often overlapping on multi-element plots (e.g. Henrichs et al., 2018). Similarly neither does apatite from high-pressure lithologies (e.g. blueschists and eclogites) exhibit distinguishing characteristics that consistently mark them apart from apatite from other metamorphic grades (e.g. El Khor et al., 2009; Henrichs et al., 2018). As more data are published on apatite compositions from metamorphic lithologies it may in future become possible to statistically discriminate apatite from different metamorphic grades and protolith types. Recent work by Henrichs et al. (2019) suggests that neoblastic apatite from Alpine greenschist-facies and lower amphibolite-facies pelites may be separately discriminated according to their geochemistry.

Apatite halogen/hydroxyl content of the Z-site in the apatite lattice can be an important control on whether apatite re-crystallises during metamorphism, as changes in fluid-composition in the metamorphic environment can be responsible for dissolution and reprecipitation of apatite with a halogen/hydroxyl composition in equilibrium with fluid (Kusebauch et al., 2015). In metamorphic rocks, recrystallized or reprecipitated apatite is generally dominated by the fluorapatite component (Spear and Pyle, 2002), with fluorine content increasing with increasing metamorphic grade, reflecting the depletion of more fluid-mobile chlorine relative to less fluid-immobile fluorine during metamorphic reactions and fluid extraction (Kusebauch et al., 2015). Apatite in metamorphic lithologies also typically exhibits relative Sr, Eu and Pb<sub>c</sub> enrichment, and relative depletion in the other REYs and Th compared to igneous apatite (Henrichs et al., 2018; Nishizawa et al., 2005).

That metamorphic apatite from substantially different protolith types (pelites vs mafic igneous rocks) is chemically indistinguishable (e.g. El Khor et al., 2009; Henrichs et al., 2018) is surprising, but can be attributed to ubiquitous processes which most low- to medium-grade metamorphic rock types at regional metamorphic pressures experience, and that in each case will ultimately render the resulting apatite REY- and Th-poor. Firstly, in most low- to medium-grade pelites and metabasites, apatite dissolution-reprecipitation or neocrystallization occurs as monazite crystallizes (pelites), and/or epidote or allanite is forming (pelites and metabasites). Epidote-group mineral growth is ubiquitous in sub-greenschist to lower amphibolite-facies metabasites, with Ca-feldspar growing at the expense of epidote at amphibolite facies conditions (Grapes and Hoskin, 2004). In metapelites and meta-marls there is a more complicated relationship between the epidote-group minerals and monazite. Monazite growth occurs below c. 440 °C, and epidote (allanite and clinzoisite) replaces monazite above that temperature. In metapelites epidote is once-again replaced by monazite at temperature

above c. 600 °C, whereas in meta-marls epidote remains stable above that temperature (according to the CaO/Na<sub>2</sub>O of the whole-rock, Janots et al., 2008). Whichever of these phases are preserved, however, in either meta-mafic or metapelitic lithologies the effect on cogenetic apatite will be the same. Both monazite and epidote/allanite are capable of incorporating significant proportions of the actinides and REEs in their crystal structures (e.g. Frei et al., 2004), and can control the whole-rock budgets of those elements (Janots et al., 2008). In such cases reprecipitated apatite may have its REE and actinide budgets scavenged by cogenetic epidote/allanite and/or monazite growth (e.g. Harlov, 2015), while neocrystalline apatite will consequently grow in a REE- and actinide-depleted chemical environment. The co-occurrence of REE- and actinide-rich epidote and REE- and actinide-poor apatite has been described in-situ from metamorphic rocks (Henrichs et al., 2018, 2019). Secondly, metamorphic apatite may form as a product of P-bearing K-feldspar dissolution during greenschist-facies albitization reactions according to the ‘berlinite’ reaction as proposed by London (1992):



Liberated P<sup>5+</sup> can be used to crystallise apatite, especially as metasomatic fluids are often OH<sup>-</sup>, Cl<sup>-</sup> and F<sup>-</sup> rich. Accordingly, neocrystalline apatite formed during this reaction inherits P, Sr and Eu from the precursor K-feldspar (e.g. Broska et al., 2004), but is devoid of the actinides and the REYs (apart from Eu) as they are not commonly substituted into K-feldspar in appreciable amounts. Thirdly, dissolution-reprecipitation processes in apatite can provide sufficient REY, Th and P necessary to precipitate monazite and xenotime (which incorporate REYs and Th as major elements) along fractures, cleavage planes, or around the apatite grain boundary, rendering the resulting apatite devoid of those elements (Harlov, 2011; Zirner et al., 2015). Dissolution-reprecipitation causes the total reorganisation of the crystal lattice (i.e. including Ca and PO<sub>4</sub> groups) with reprecipitation of apatite on the grain surface (e.g. Kusebach et al., 2015), or in internal voids within the apatite created by dissolution-reprecipitation (Harlov, 2015). The dissolution-reprecipitation mechanism thus provides Th, P and REE for the growth of epitaxial or interior (i.e. included within apatite) grains of monazite and xenotime.

**2.1.2.1. Refractory apatite in metamorphic rocks.** In metamorphic rocks, it is important to be able to distinguish between pre-existing apatite inherited from the protolith (e.g. detrital apatite in a metasedimentary rock, or igneous apatite phenocrysts in a meta-igneous rock) from neoblastic apatite that has grown in the metamorphic rock itself. In low-grade metamorphic rocks, both inherited apatite and metamorphic apatite can co-exist, as seen for example in lower-greenschist facies metagreywackes in the Haast schist of the New Zealand Southern Alps where apatites with igneous compositions are preserved (Henrichs et al., 2018). Both Henrichs et al. (2018) and Nutman (2007) have shown that in metasedimentary rocks, detrital apatite is typically consumed by the upper-greenschist facies, with new growth of apatite likely due to a coupled dissolution-reprecipitation process (e.g. Harlov, 2015). In situations where apatite is hosted in ‘unreactive’ lithologies (such as anhydrous coarse-grained plutonic lithologies, or monomineralic metasedimentary lithologies (such as marbles or quartzites), it is possible that detrital apatite will persist to higher metamorphic grades, similar to the behaviour of rutile hosted in unreactive assemblages (Luvizotto et al., 2009). Such behaviour has been observed by Schneider et al. (2015), who analysed apatite U–Pb ages in Variscan orthogneisses which have experienced Alpine 450–575 °C overprinting in the Tauern window in Eastern Austria. The apatite U–Pb ages in these meta-granitoid orthogneisses were dispersed, with two peaks in the U–Pb age spectrum corresponding to the age of igneous emplacement and Alpine MT-LP orogenesis (although a

continuous U–Pb age-distribution between these populations was present). This implies that some Tauern apatites retain refractory U–Pb age information to temperatures much higher than suggested by Pb-diffusion models in apatite (c. 350–475 °C, Cherniak, 2010).

**2.1.2.2. Metasomatic apatite geochemistry.** Apatite formed during metasomatic processes (e.g. late stage fluid alteration in granites) often has trace-element compositions that are indistinguishable from low- to medium-grade metamorphic apatite, i.e. low REE contents, high Ca, F and Sr contents, and minor Eu-anomalies (Chakhmouradian et al., 2017 and sample 13 therein). These apatites are hence considered here alongside low-grade metamorphic apatite (as part of the “LM” group on diagrams, e.g. Fig. 2), as in provenance samples metasomatic apatite will be indistinguishable from low-grade metamorphic apatite. Dissolution-reprecipitation reactions can occur during the cooling of igneous rocks for example, especially in fluid-rich systems such as pegmatites, where late-stage fluids may catalyse the precipitation of REY-poor apatite, monazite and xenotime from REY-rich primary igneous apatite (e.g. Harlov, 2011), especially locally along fluid-pathways in the rock. Altered portions of granites should therefore be avoided if trying to obtain U–Pb ages from igneous rocks, as REY-poor apatite is more likely to contain lower U and radiogenic Pb (Pb\*) and higher Pb<sub>c</sub> than primary igneous apatite (e.g. Henrichs et al., 2018). Conversely, REY-poor apatite thus may be a useful indicator mineral of ore-mineralisation in igneous terranes (Glorie et al., 2019; Mao et al., 2016), as in detritus the chemical signature may be useful as vector for the presence of metasomatised rocks in the hinterland.

### 2.1.3. High-grade metamorphic and leucosome apatite

At high-metamorphic grades, mineral assemblage equilibration rates are typically sufficiently fast that samples are often in chemical equilibrium on the scale of a thin section or hand sample; dispersed apatite trace element spectra are typically not encountered in such rocks (e.g. Bingen et al., 1996; Bea and Montero, 1999; Nutman, 2007; Henrichs et al., 2018). This also indicates that all apatite present in the protolith before metamorphism occurred has long since been consumed or overprinted (high-grade apatite at c. < 750 °C can accommodate solid-state exchange of REEs; Cherniak, 2010). Apatite in higher-grade metamorphic rocks is almost universally fluorapatite (Spear and Pyle, 2002), and also typically contains higher REE- and actinide-abundances than apatite from lower-grade metamorphic lithologies (“HM” panel on Fig. 2).

Bingen et al. (1996) studied an amphibolite to upper granulite-facies transect through high-K calc-alkaline gneisses. The REE, Th and U contents of apatite increase progressively with increasing grade. Following dissolution of allanite, hornblende and titanite at the Cpx-in isograd, the MREE and HREE in apatite increase, and upon the dissolution of monazite at the Opx-in isograd the LREE- and Th-contents of apatite increase significantly. Biotite-breakdown at the Opx-in isograd and the consequent release of apatite-stabilising F may also promote the migration of REE into the apatite lattice in the form of NaF complexes (Krenn et al., 2012). Apatite from the Opx-grade rocks has REE-contents and ratios indistinguishable from granitoid apatite (e.g. Chu et al., 2009)

As apatite is unstable in igneous melts (Piccoli and Candela, 2002), in rocks that undergo anatexis apatite is consumed into the melt or fluid, from which apatite will then crystallise upon cooling. P is thus strongly partitioned into melt or fluid compared to restite (Bea and Montero, 1999). Leucosome apatite typically presents geochemical signatures similar to that of S-type granitoid apatite (Fig. 2), with low Th/U, low La/Ce and flat chondrite-normalised REE-profiles (e.g. Bea and Montero, 1999; Nutman, 2007; Henrichs et al., 2018), although generally with weaker negative Eu-anomalies than S-type granite apatite (Fig. 2). This may be due to peritectic apatite growth in the absence of (Eu-sequestering) feldspar. In both high-grade pelites that have experienced anatexis (e.g. anatetic pelites from Nutman, 2007) and those

that have not (e.g. high-grade Peruvian and Cycladic paragneisses from [Henrichs et al., 2018](#)), Th is strongly depleted relative to U, and the LREE are slightly depleted. [Nutman \(2007\)](#) ascribes Th and LREE depletion to the cogenetic growth of monazite, which is similar to the paragenesis and composition of apatite from S-type granitoids documented in other studies (e.g. [Hsieh et al., 2008](#)). In contrast to leucosome apatite, apatite in restites, especially those that crystallise garnet, exhibits depletion in HREE and Y (e.g. [Bea and Montero, 1999](#)), thus more closely resembling apatite in mafic igneous lithologies.

#### 2.1.4. Authigenic and chemical-precipitate apatite

Apatite is found as a chemical precipitate in some P-bearing chemical sediments, such as banded iron formations (e.g. [Joosu et al., 2016](#) and references therein) and phosphorites where it may instead occur as the cryptocrystalline apatite phase collophane and carbonate-apatite (francolite). Additionally, apatite may grow during diagenesis (e.g. [Bouch et al., 2002; Vermeesch et al., 2009](#)), and may even occasionally occur as the major cement phase in detrital sediments (e.g. [Gall et al., 2017; Joosu et al., 2016](#)). Apatite grows in sediments due to the liberation of P from organic matter decay, and from the liberation of P adsorbed onto clay-mineral surfaces. While the process of liberation of organic-P can begin within the first five metres beneath the sediment-water interface as seen in modern sediment samples (e.g. [Ruttenberg and Berner, 1993](#)), adsorbed and early authigenic P is likely only to be mobilised under deep burial diagenesis with large apatite rims typically reported at depths below c. 3 km in the North Sea (e.g. [Bouch et al., 2002](#)).

In studies of authigenic apatite in the geological record,  $\Sigma$ REE contents vary substantially (e.g. [Bouch et al., 2002; Joosu et al., 2015, 2016](#)), but the topology of the chondrite-normalised REE patterns are distinct compared to other categories of apatite (Authigenic apatite "AUT" [Fig. 2](#)). While in some well-preserved sections marine authigenic apatite may preserve REE-abundances, negative Ce-anomalies and distinct Y/Ho ratios (e.g.  $Y/Ho > 35$ ) ([Lawrence and Kamber, 2006](#)) characteristic of the seawater REE-signal (e.g. basal Cambrian phosphorites from the Meischucun formation in southern China; [Shields and Stille, 2001](#)), diagenetic processes in many cases overprint this signal ([Shields and Stille, 2001](#)). Consequently, negative Ce-anomalies are less pronounced and  $\Sigma$ REE contents increase (especially the MREE) with increasing alteration. Apatite with pronounced negative Ce-anomalies is thus characteristic of an authigenic origin, but as this signal may often be obscured or destroyed during diagenesis, the absence of a seawater-like Ce-anomaly therefore does not preclude an authigenic origin.

In altered authigenic apatite that no longer preserves seawater-like REY signatures, the sources for REY- and actinide-rich (e.g. [Bouch et al., 2002; Vermeesch et al., 2009](#)) overgrowths on apatite is probably the dissolution of other REY- and actinide-bearing phases in detritus ([Bouch et al., 2002](#)), most probably phases such as garnet, titanite, allanite and epidote which are unstable during burial diagenesis ([Morton and Hallsworth, 1999](#) and references therein). In some cases apatite cementation may even be dated by the apatite fission-track (AFT) or U–Pb methods to provide timing constraints on the diagenetic history (e.g. [Gall et al., 2017; Malusà and Fitzgerald, 2019](#)).

#### 2.1.5. Summary of apatite compositions

The preceding sections described the chemistry of apatite in terms of the REEs and other trace elements from various major bedrock groups. To generalise trends seen in apatite from these categories, there are at least four factors that show major differences between the various groups; some of these differences have been long recognised and are well documented in the literature (e.g. [Fleischer and Altschuler, 1986](#)).

Firstly, total REE content is lowest in low-grade metamorphic apatite (e.g. [El Khor et al., 2009](#)) and increases with increasing grade such that in very high-grade rocks, the apatite REE content is indistinguishable from that of igneous apatite (e.g. [Bingen et al., 1996](#)).

Igneous apatite has reasonably similar REE contents regardless of whether the host lithology has mafic or felsic chemistry (for example compare the REE content in apatite in felsic and adakitic rocks from [Chu et al., 2009](#)). The exception is apatite in alkali-rich rocks ([Fig. 2](#)), which is ultra-enriched in REE (e.g. [Zirner et al., 2015](#)). Secondly, negative Eu-anomalies are present in apatite from all bedrock types except ultramafic rocks (e.g. [Chakhmouradian et al., 2017](#)), most low-grade metamorphic rocks (e.g. [Henrichs et al., 2018](#)), and non-hydrothermal associated authigenic apatite (e.g. [Joosu et al., 2016](#)). The magnitude of the negative Eu-anomaly in igneous rocks is typically positively correlated with  $SiO_2$  content ([Fig. 2](#)). Thirdly, the Sr content of apatite is negatively correlated with  $SiO_2$  content, with the highest Sr contents observed in ultramafic rocks ([Ihlen et al., 2014](#)) and the lowest Sr contents in felsic rocks ([Sha and Chappell, 1999](#)). In metamorphic apatite, there is a link between metamorphic grade and Sr content, which is highest in greenschist- and blueschist-facies rocks ([Nishizawa et al., 2005](#)) and lowest in migmatites and granulite-facies rocks (e.g. [Nutman, 2007](#)). Lastly, the La/Lu ratio in apatite is also strongly correlated to the chemistry of the host lithology. Generally speaking, apatite in felsic igneous rocks and metamorphic rocks of all grades has chondrite-normalised (e.g. [McDonough and Sun, 1995](#))  $La^{norm}/Lu^{norm} \leq 1$ , and in all other rocks apatite  $La^{norm}/Lu^{norm}$  is  $> 1$  ([Fig. 2](#)), with the highest chondrite-normalised LREE/HREE ratios seen in apatite from ultramafic rocks (e.g. [O'Reilly and Griffin, 2000](#)).

#### 2.2. Previous provenance and correlation work employing apatite trace-element compositions

The workflow discussed below for the use of trace element composition as a single grain provenance tool is fundamental, whether in tephra or detritus, and all such studies must employ some variation of the following methodology. Firstly 'knowns' must be analysed or referenced; these are crystals of the mineral of interest from bedrock samples (or well characterised reference sections in tephra correlation studies) to which detritus or tephra can be compared. If these grains of known composition display consistent and significant (i.e. resolvable) variations that can be linked to either the host rock chemistry or their position in the regional volcanic stratigraphy, then it is feasible to construct a bedrock or tephrochronology database for the mineral of interest. This database of known compositions can subsequently be used as a reference to compare unknown grains of the same mineral against, and which can then be used to assign unknowns based on their affinity to the reference database of known compositions. This workflow has held since the first single-grain compositional and isotopic provenance studies, such as those of garnet compositional variations by [Morton \(1985\)](#) and of zircon Hf-isotope characterisation by [Owen \(1987\)](#). This workflow is also the basis of detrital feldspar Pb–Pb analysis (e.g. [Tyrell et al., 2007](#)).

That apatite trace element composition is at least partly controlled by the host rock chemistry has been long recognised (e.g. [Fleischer and Altschuler, 1986](#)), as has its potential as a provenance/correlation tool. [Samson et al. \(1995\)](#) employed apatite chemistry as a correlative tool in heavily weathered tephra in which the primary glass phases had been completely altered (e.g. K-bentonites). REE, Mg, Fe, Cl and Sr-isotope chemistry were used to correlate K-bentonite layers in the North American continent using single apatite grains; however, REE-composition was considered to be of only moderate usefulness, perhaps due to similarities in the REE chemistries of the tephra parent magmas. Use of apatite trace element composition as a correlative tool in weathered tephra sections has continued since then, both in studies of ancient tephras (e.g. [Carey et al., 2009; Emerson et al., 2004; Sell et al., 2015](#)) and in weathered Cenozoic tephra samples (e.g. [Sell and Samson, 2011](#)).

[Dill \(1994\)](#) was the first major application of apatite REE and actinide chemistry as a *detrital* provenance tool. [Dill \(1994\)](#) achieved this by characterising the REE and actinide chemistry (and U–Pb ages) of

potential apatite-bearing source rocks to Permo-Triassic clastic rocks in southern Germany, and then seeking to recognise similar chemistries in the REE and actinide contents of detrital apatite in this Permo-Triassic clastic succession. The analysed bedrock apatites were diverse in their chemistry and thus formed the basis of a useful (if somewhat limited) bedrock reference library. Provenance determinations were made using chondrite-normalised REE-pattern matching and the Th/U characteristics of the bedrock samples and apatite detritus. However, analytical constraints compromised the feasibility of using the method of Dill (1994) more widely, as detrital samples were measured in bulk by thermal ionisation mass spectrometry and thus represented mixes both of all detrital populations and of diagenetic apatite components, thus significantly limiting the usefulness of the method.

Morton and Yaxley (2007) successfully applied apatite trace-element analysis to single detrital grains by employing laser-ablation quadrupole inductively coupled plasma mass spectrometry (LA-Q-ICP-MS). This greatly expanded the utility of apatite trace element analysis compared to the bulk thermal ionisation method applied to detrital apatite by Dill (1994), permitting the linking of individual grains to individual sources. The expansion in available data on (mostly igneous) bedrock apatite compositions by that time (e.g. Bea and Montero, 1999; Belousova et al., 2001; Belousova et al., 2002a,b; Bingen et al., 1996; Sha and Chappell, 1999) was aided by the increasing availability of high-throughput LA-Q-ICP-MS instrumentation. The development of tools from those data, such as discrimination schemes for apatite from igneous lithologies, aided determinations of apatite provenance and since then other studies have successfully employed similar methodologies (e.g. Abdullin et al., 2016). These discrimination schemes include the pioneering work of Fleischer and Altschuler (1986) for discriminating acidic, intermediate and alkaline igneous apatite ( $\text{La}/\text{Nd}$  vs  $[\text{La} + \text{Ce}]/\Sigma\text{REE}$ ); apatite Th/U diagrams as first applied by Dill (1994); and  $\text{Sr}$  vs  $\text{Y}$ ,  $\text{Sr}$  vs  $\text{Mn}$ ,  $\text{Y}$  vs  $\text{Eu}/\text{Eu}^*$ , and  $\text{Ce}/\text{Yb}$  vs  $\Sigma\text{REE}$  diagrams for the discrimination of apatite from a variety of igneous rocks as first proposed first by Belousova et al. (2002a,b). Belousova et al. (2002a,b) also applied machine-learning methods to their dataset, using a Classification And Regression Tree (CART) analysis, which is able to assign a likely provenance to unknown detritus based upon the characteristics of the input database of known composition.

As the apatite discrimination diagrams and models developed by Belousova et al. (2001, 2002), Dill (1994) and Fleischer and Altschuler (1986) were largely developed for igneous apatite discrimination, these methods perform relatively poorly when non-igneous apatite detritus or detritus from less common igneous rocks is included. This issue was described by Morton and Yaxley (2007), who noted plentiful probable misclassifications of apatite detritus in their samples, and thus determined that (ibid, p.340) “acquisition of a more comprehensive set of apatite-bearing lithologies (including other igneous lithologies and, perhaps more importantly, metamorphics) would help to refine the approach”. Large datasets of apatite trace element compositions from metamorphic rocks and ultramafic and alkali-rich igneous rocks have largely been unavailable until relatively recently (e.g. Chakhmouradian et al., 2017; El Khor et al., 2009; Henrichs et al., 2018, 2019; Hsieh et al., 2008; Nishizawa et al., 2005; Zirner et al., 2015), meaning that further development of apatite composition as a provenance tool is only now becoming possible.

Isotopic tracing of apatite detritus is another provenance technique that has been developed over the last decade. These studies require the use of MC-ICP-MS and employ the Sm–Nd system (e.g. Carter and Foster, 2009; Foster and Carter, 2007; Henderson et al., 2010). It has been demonstrated that apatite Nd isotopic compositions are faithful recorders of the Nd-isotope systematics of their host lithology, making it a useful provenance tool once source characterisation has been undertaken (e.g. Foster and Carter, 2007).

Many recent apatite provenance studies have employed multi-proxy approaches. These include combining trace element or isotope analysis of apatite with fission-track analysis of the same grains (e.g. Malusà

et al., 2017; Foster and Carter, 2007; Carter et al., 2018); and combining detrital apatite trace element and U–Pb analysis of the same grains in the same analytical session (e.g. Gillespie et al., 2018; Kenny et al., 2019; Mark et al., 2016). Other areas of development include the application of compositional statistics to apatite trace element data (e.g. O'Sullivan et al., 2018), as has previously been applied to sedimentary provenance studies more generally, especially in heavy mineral analysis (e.g. Aithcinson, 1982; von Eynatten et al., 2003; Weltje, 2012). Provenance determinations employing the halogen content of apatite is another area of recent interest for use as a provenance proxy, and in a suitably characterised hinterland has the potential to distinguish different granitic bodies in plutonic suites when integrated with apatite trace element compositional data (Ansberque et al., 2019). Recent work has also developed apatite composition as a tracer of ore-genetic processes, including the assembly of large geochemical databases (Mao et al., 2016). As previously discussed, apatite trace element chemistry (REE, Sr, halogen chemistry etc.) is sensitive to fluid alteration (e.g. Kusebauch et al., 2015), meaning apatite composition may be used to track the geochemical footprints of metallogenetic fluids (Glorie et al., 2019).

Apatite inclusions in detrital zircon are also a useful provenance tool. It has been demonstrated that apatite inclusions are faithful recorders of the composition of matrix apatite and provide the ability to ascertain the chemistry of melt in which the host zircon crystallised (e.g. Bruand et al., 2016; 2017). This is especially useful, as for provenance purposes the trace element chemistry of zircon is typically less sensitive than apatite to the parent melt geochemistry (e.g. Hoskin and Ireland, 2000), with some notable exceptions for certain lithologies such as the oceanic crust (e.g. Grimes et al., 2007).

The utility of apatite trace element compositions as a provenance tool can thus be seen to have improved with the increasing amount of bedrock information available to the community (aided by increasing availability of LA-ICP-MS instrumentation). These data permit the compilation of datasets and the development of discriminatory tools that ultimately permits multi-dimensional analysis of apatite provenance. Large published datasets of apatite trace element compositions (including of previously overlooked rock types), such as that of Mao et al. (2016) who published individual analyses of c. 1000 bedrock apatite grains, are of critical importance to increasing the utility of apatite composition as a provenance tool. It is also key that future studies publish all individual spot analyses (e.g. Mao et al., 2016) instead of “representative means” in order to allow more robust statistical treatment of those datasets.

### 2.3. Geochronology/thermochronology of apatite

Apatite often contains significant concentrations of the radioisotopes U and Th and thus can be employed as a geochronological or thermochronological tool. There are three commonly applied geo- and thermo-chronometric methods employed to apatite and which are relevant to detrital applications. In order of highest to lowest temperature sensitivity, these are the apatite U–Pb, apatite fission track (AFT), and apatite U/Th-He techniques respectively.

Apatite U–Pb is a high temperature geochronological tool, and typically provides data on the age of apatite crystallization, or the cooling of apatite through the temperature window for partial retention of Pb. Pb accumulates in the apatite lattice as the ultimate decay product of the  $^{238}\text{U}$ ,  $^{235}\text{U}$  and  $^{232}\text{Th}$  decay series ( $^{206}\text{Pb}$ ,  $^{207}\text{Pb}$  and  $^{208}\text{Pb}$  respectively). The temperature sensitivity of the U–Pb system in apatite is governed by the diffusion of Pb, with the partial retention zone for Pb determined at c. 350–475 °C based on diffusion experiments (Cherniak, 2010), though individual rock samples in natural settings that have been heated to much higher temperatures (up to c. 575 °C) can preserve ante-metamorphic ages in some cases (Schneider et al., 2015). Moreover, as apatite is very prone to dissolution-reprecipitation during metamorphism (Harlov, 2015), the U–Pb age of apatite in

metamorphic rocks may thus reflect the most recent reordering of the crystal lattice, rather than recording processes linked to thermally-activated volume diffusion of Pb (cf. Dodson, 1973). For U–Pb apatite analysis, grains with minor defects and inclusions can be analysed by LA-Q-ICP-MS, as data reduction packages such as Iolite (Paton et al., 2011) permit exclusion of the inclusion in the time-resolved U–Pb signal. U–Pb dating of minerals by LA-Q-ICP-MS is now a cheap, rapid and effective dating tool (e.g. Spencer et al., 2016). When there is a sufficient spread in  $\text{U}/\text{Pb}^*$  ratios to yield well-constrained concordia intercept ages, a precision better than 1% ( $2\sigma$ ) is possible for Phanerozoic apatite samples (e.g. typically 20–30 analyses from a magmatic or metamorphic rock), with a precision better than 2% possible even with Palaeogene age apatites (e.g. Chew et al., 2014). The factors that govern whether a given unknown detrital apatite grain may be accurately and precisely dated by the U–Pb method are threefold. Firstly, the grain must have abundant U and Th to produce sufficient  $\text{Pb}^*$  to yield favourable  $\text{Pb}^*/\text{Pb}_c$  ratios (i.e. the amount of Pb produced by radiogenic ingrowth [ $\text{Pb}^*$ ] must not be dwarfed by Pb present when the grain crystallised [common Pb =  $\text{Pb}_c$ ]). Secondly, the age of the grain itself, as older grains are clearly more amenable to dating due to the longer duration for  $\text{Pb}^*$  in-growth; and thirdly the grain must contain low initial  $\text{Pb}_c$  concentrations, or else  $\text{Pb}^*$  in-growth will never become a significant proportion of the total Pb in the grain, even with high initial U abundances. Grains that have very high  $\text{Pb}_c/\text{Pb}^*$  ratios are thus excluded from U–Pb age density plots as they do not produce meaningful data, which undoubtedly introduces a lithological bias as apatite U contents vary according to lithology (discussed in section 3.1). Apatite U–Pb dating by LA-Q-ICP-MS also permits simultaneous acquisition of a large number of trace elements (e.g. Kenny et al., 2019), which can be employed in apatite compositional analysis, while U concentration data can also be used for AFT analysis in apatite double-dating (AFT and U–Pb) studies (Chew and Donelick, 2012).

AFT is a low-temperature thermochronology tool, with widespread application in thermal modelling of basins (e.g. Fernandes et al., 2015), estimation of exhumation rates (e.g. Cogné et al., 2014; Malusà et al., 2005) and determination of fault slip rates (e.g. Wallis et al., 2016). It can also be employed in detrital provenance studies (e.g. Chew and Donelick, 2012; Resentini and Malusà, 2012) if the samples remained below the temperature of the apatite partial annealing zone (60–110 °C) following deposition (Hurford and Carter, 1991). Fission tracks are produced in minerals from the spontaneous fission of radionuclides (overwhelmingly  $^{238}\text{U}$ ) hosted in the mineral lattice (Hurford, 2018). These fission events produce linear defects in the lattice of U-bearing minerals that are enlarged using a standardized chemical etching process so they can be observed under an optical microscope. A fission track age provides an estimate of the time that has elapsed since the mineral cooled through the apatite partial annealing zone (PAZ). At temperatures above the PAZ (110 °C ± 10 °C, Gallagher et al., 1998), there is sufficient energy to completely anneal (or remove) fission tracks via thermally activated diffusion of the relocated ionic species in the lattice. At temperatures below 60 °C there is insufficient energy to repair spontaneous fission tracks, while within the PAZ at temperatures between 60 and 110 °C, apatite fission tracks will be partially annealed (e.g. Gleadow and Duddy, 1981). The fission track age and fission track length distribution of an apatite crystal is thus a function of temperature and time, and can be combined to construct time–temperature paths by inverse and/or forward modelling of the fission track age and length data (e.g. Ketcham, 2005). Grain composition (e.g. Z-site composition) and crystallography also controls annealing behaviour (e.g. Barbarand et al., 2003), meaning that characterisation of the halogen component of an apatite grain can be used as a kinetic parameter to help constrain the annealing behaviour.

Apatite (U/Th)-He dating is a low temperature thermochronology tool with a suite of applications similar to those of apatite fission-track dating studies, such as estimating rates of exhumation and fault-slip (e.g. Stockli et al., 2000; Ricketts et al., 2016), but which typically

provides information about even lower temperature portions of the thermal history (Ehlers and Farley, 2003). Apatite (U/Th)-He dating has also been employed in provenance studies (e.g. Zattin et al., 2012), with specific applications including the quantification of catchment-scale erosion rates (e.g. Stock et al., 2006). Accumulation of  $^4\text{He}$  in minerals occurs due to the radioactive decay of  $^{238}\text{U}$ ,  $^{235}\text{U}$  and  $^{232}\text{Th}$  and their intermediate daughter products (though  $^{147}\text{Sm}$ , an abundant trace element in apatite, also contributes  $^4\text{He}$ ), a process by which an alpha particle (a  $^4\text{He}$  nucleus) is released (Ehlers and Farley, 2003). Helium atoms have the smallest atomic radius of any element (Clementi et al., 1967) and are not lattice-bound, being present interstitially in the mineral lattice, and He is thus a metastable element in the minerals in which it accumulates. Helium is able to quickly diffuse out of the apatite lattice at temperatures above c. 70 °C, which typically corresponds to depths of c. 1–3 km depending on the geothermal gradient (Wolf et al., 1996). Detrital apatite grains must therefore not have experienced significant heating or burial after deposition in order to be employed in provenance determinations employing (U/Th)-He age data. For He analysis, apatite grains should preferably be euhedral, must be free of inclusions (as inclusions such as zircon may contribute ‘parentless’ He), and also be free of major defects which may act as pathways for the escape of He from the crystal (Farley, 2002). The distribution of He in an apatite crystal is also related to the distribution of U, Th and Sm. Crystal rims enriched in these radioisotopes may lose a greater proportion of He to out-diffusion; LA-ICP-MS mapping of grains to characterise the U, Th and Sm distribution can lead to very different interpretations of time–temperature paths (Farley et al., 2011). Domains of radiation damage can inhibit He diffusion leading in some cases to (U/Th)-He dates that are older than AFT dates, although this behaviour can be modelled (e.g. Flowers et al., 2009).

From a historical viewpoint, the first forays into phosphate chronometry were made by Strutt (1908), who dated phosphatic nodules and phosphatised bones and teeth by the (U/Th)-He method. The method was eventually abandoned as a geochronometer as evidence mounted (e.g. Hurley, 1954) that minerals were highly prone to loss of radiogenic He. The first apatite U–Pb ages were published in the 1950s (e.g. Larsen et al., 1952), and apatite fission track (AFT) thermochronology was first developed by a series of pioneering studies in the 1960s (e.g. Fleischer and Price, 1964; Naeser, 1967; Wagner, 1968). U–Pb TIMS dating of apatite was first undertaken in the 1970s by Oosthuizen and Burger (1973), and although that study yielded near-concordant apatite U–Pb age data, it should be noted they were Archaean samples with significant in-growth of radiogenic Pb. Subsequent studies have shown that apatite often yields strongly discordant U–Pb data due to high  $\text{Pb}_c/\text{Pb}^*$  ratios and therefore requires a common-Pb correction in order to produce useful age data (e.g. Thomson et al., 2012). Apatite U–Pb dating therefore remained a niche application for several more decades. In the 1980s the apatite (U/Th)-He method was re-investigated and established as a useful tool for thermochronometry (Zeitler et al., 1987), rather than for geochronometry as had previously been attempted. Apatite single-grain U–Pb geochronology only became possible with the advent of rapid in situ micro-beam dating techniques (e.g. secondary ionisation mass spectrometry, SIMS and LA-ICP-MS), along with the concomitant development of apatite U–Pb age-standards and data reduction schemes employing  $^{207}\text{Pb}$ - or  $^{204}\text{Pb}$ -based  $\text{Pb}_c$  corrections to age standards and unknowns (Thomson et al., 2012; Chew et al., 2014). Modern methodologies in AFT analysis employ forward and inverse modelling of combined track length and AFT age data to construct time–temperature histories (e.g. Gallagher, 2012; Ketcham, 2005).

It is now possible to combine geo/thermo-chronological methods in detrital apatite, and double-dating (e.g. Cogné et al., 2014; Glorie et al., 2017) and even triple-dating (Carrapa et al., 2009; Zattin et al., 2012) studies can be performed on the same grains, although this approach does require a much greater input of labour and the use of a range of analytical equipment.

### 3. Methodology

#### 3.1. Data Synthesis

A central pillar of this paper is the synthesis of apatite trace element data published over the past three decades from twenty-two papers (Bea et al., 1994; Bea and Montero, 1999; Belousova et al., 2001; Belousova et al., 2002; Chakhmouradian et al., 2017; Chu et al., 2009; Dill, 1994; El Khor et al., 2009; Henrichs et al., 2018; Hsieh et al., 2008; Ihlen et al., 2014; Joosu et al., 2015; Joosu et al., 2016; Mao et al., 2016; Nishizawa et al., 2005; Nutman, 2007; O'Reilly and Griffin, 2000; Sha and Chappell, 1999; Shields and Stille, 2001; Tang et al., 2012; Tollari et al., 2008; Zirner et al., 2015). This dataset (illustrated on Fig. 2) incorporates apatite from 351 separate global bedrock samples to provide an empirical record of apatite compositions. The bedrock samples range from S-type granites to I-type granitoids, alkali-rich igneous rocks, mafic igneous rocks, ultramafic igneous rocks, high-grade and low-grade metamorphic rocks of diverse protolith type, and authigenic and fossil apatite. This dataset is provided as a supplemental file (S1), and is also available on the pangaea.de archive (<https://doi.pangaea.de/10.1594/PANGAEA.906570/>). It is our intention that this dataset will be continuously updated in future as more bedrock apatite data are published.

In order to usefully plot and compare the published data, the studies must have analysed the full suite of elements selected for the biplots and PCA used in this study (Sr, La, Nd, Sm, Eu, Gd, Y and Lu; note that Sm, Eu and Gd were only required for the PCA analysis). These are all trace elements that occur in high but variable (single-ppm to parts-per-thousand) concentrations in apatite, and were thus considered to be potentially useful discriminators and that are easily measured using standard quadrupole ICP-MS instruments. The exclusion of some potentially useful apatite datasets characterising lithologies not included in the dataset (e.g. the high grade lower-crustal orthogneisses analysed by Bingen et al., 1996) stems from the absence of key elements in those (usually older) published datasets. Likewise, the exclusion of elements with potential discriminatory power such as U, Th and Mn, is also necessary, as too few published datasets include those elements. Additionally, not all the REEs were plotted as no useful additional information is acquired by plotting all 14 REEs, rather than by selecting representative light, middle and heavy rare earths. Quality screening was applied to the bedrock apatite database; igneous and authigenic bedrock samples that authors described as metasomatically altered were excluded, as were igneous samples that were identified as having experienced subsequent metamorphism (e.g. apatite from the Sybella and Kalkadoon plutons in the study of Belousova et al., 2001). Additionally, any samples that exhibited substantial trace-element dispersion between apatite grains were omitted as these samples can reasonably be expected to contain either detrital grains or are rocks that have experienced partial metamorphic alteration and thus defy simple categorisation as required by our methodology (e.g. sample LT2 of Henrichs et al., 2018, which contains both low-grade metamorphic and detrital apatite populations).

The bedrock types on the various biplots presented in this study were initially chosen according to their description by the authors of the respective cited papers. However, as some closely related groups almost completely overlapped on biplots, the lithologies were combined into broader lithological groupings in an iterative process. For example, as apatite from carbonatites, pyroxenites and lherzolites always overlap on biplots, they are grouped as "UM" for ultramafic apatite; likewise, mafic I-type granites (i.e. low ASI, non-peraluminous granites, e.g. Chu et al., 2009; Hsieh et al., 2008), granodiorites and mafic igneous apatite significantly overlap and are therefore plotted together as a group called "IM" (for mafic I-type and mafic igneous apatite). While the logic for constructing these larger categories is partly circular, the categories are all considered to be sensible and conservative by the authors given the current state of knowledge of apatite geochemistry, as

demonstrated in the introduction to this paper and as shown in Fig. 2.

Due to the differences in data reporting in the available literature, a mix of median values and spot values are used. Where available, spot data were preferably used. The data are thus weighted towards studies that published the individual apatite analyses for each analysed rock (e.g. Mao et al., 2016; Zirner et al., 2015; Henrichs et al., 2018 amongst others). We have greater confidence in those studies that do publish all data as they permit more comprehensive interrogation of the trace element systematics, so we do not view this as a significant negative bias.

#### 3.2. Principal components analysis (PCA), biplots, and support vector machines (SVM) overview

In large datasets efficient data visualisation is paramount, as the volume of data points is too large to be conveniently assessed on a table or on a multi-element spidergram (Fig. 2). This is particularly the case when hundreds or thousands of data points corresponding to unknown detritus are subsequently added. Additionally, in order to adequately interrogate the data, several variables (elemental abundances or elemental ratios) need to be employed simultaneously. Consequently, principal component analysis (PCA) is used to initially separate and visualise the bedrock dataset (Fig. 3a), as PCA is suitable for the visualisation of many data points with multiple dimensions. The results of this PCA are then used to determine the most useful set of element ratios and abundances for maximum category separation. Biplots of these ratios and abundances (i.e. those derived from the information provided by PCA) are then demonstrated using three previously published detrital case studies, where existing provenance information (e.g. U–Pb apatite age data) has resulted in some non-unique provenance interpretations. Subsequently, the information on that biplot is input to a multiclass Support Vector Machine (SVM; Vapnik, 2013) in order to construct a fully reproducible categorical classification scheme for unknowns based on the bedrock samples. Spidergrams of the median values of bedrock groups used on the PCA biplots and element ratio biplots are also provided as another way to visualise and understand the apatite trace element dataset (Fig. 2).

PCA is a statistical method that has a long history of application to geological data, especially in sedimentology (e.g. Aitchinson, 1982; Webb and Briggs, 1966) that transforms (i.e. rotates and shears) a data matrix of  $n$ -dimensions in order to display the data contained in that matrix along axes showing the greatest variance. The first principal component is parallel to the axis of greatest variance in the matrix, the second principal component is orthogonal to the first and so on. As most components in a dataset may not account for a significant portion of the variance, PCA permits dimensionality-reduction in cases where the highly-ranked components account for the vast majority of the variance. PCA is an unsupervised statistical method, and user-defined categorical information has no impact upon the transformation (Kuwatani et al., 2014). The methodology employed in this paper uses specific trace elements, which are summed and subtracted from a residual ("CaPO") representing all other trace and major elements in the analysed apatite aliquot (i.e. 1,000,000 ppm). The data are transformed using a centred log-ratio (CLR) transformation before PCA transformation (Aitchinson, 1982).

Once the preferred element ratio biplot is determined, it is necessary to provide a method of categorizing unknown apatite according to predefined groups on biplot. The methodology employs a Support Vector Machine (SVM) classification. SVM is a machine-learning classifier method (e.g. Mavroforakis and Theodoridis, 2006; Vapnik, 2013) that employs user-defined groups and finds the hyperplanes (*decision-boundaries*) that define the simplest maximum separation for given tuning parameters (these define, for example, the radius of influence upon the hyperplane calculation that individual points should have). The decision-boundaries are defined by a subset of the datapoints (kernels) that best separate the user-defined categorical classes for

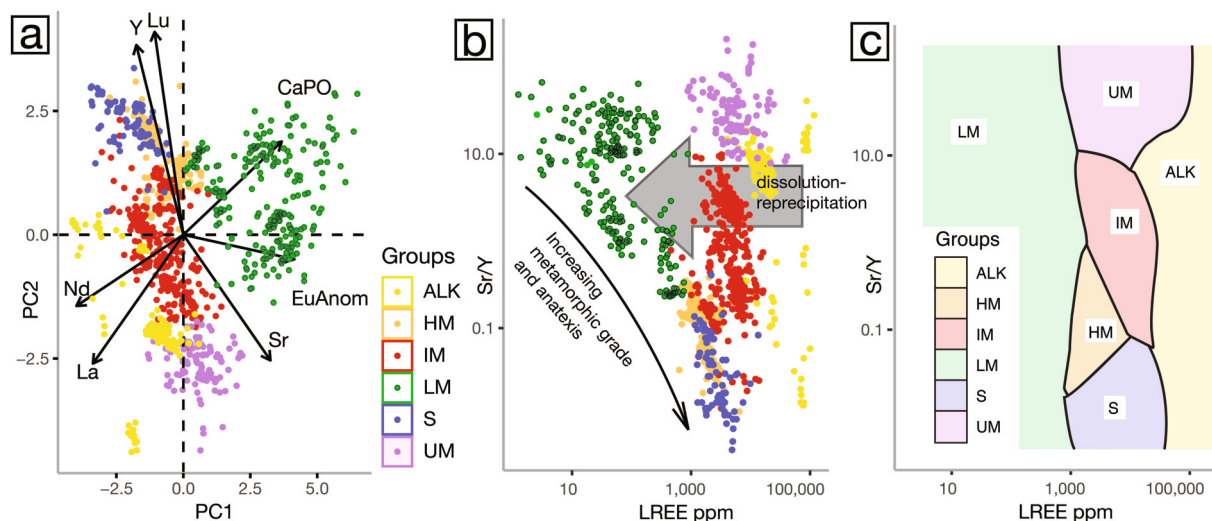


**Fig. 3.** Biplots of apatite from the bedrock apatite database. (a) An apatite bedrock PCA biplot; (b) a  $\text{Sr}/\text{Y}$  vs  $\Sigma\text{LREE}$  (defined here as  $\text{La}-\text{Nd}$ ) biplot using the same data, which produces an almost identical separation of the data (especially if rotated); (c) a support vector machine (SVM) categorisation scheme based upon the bedrock data points on  $\text{Sr}/\text{Y}$  vs  $\Sigma\text{LREE}$  biplot. Abbreviations for groups: ALK = alkali-rich igneous rocks; IM = mafic I-type granitoids and mafic igneous rocks; LM = low- and medium-grade metamorphic and metasomatic; HM = partial-melts/leucosomes/high-grade metamorphic; S = S-type granitoids and high aluminium saturation index (ASI) 'felsic' I-types; UM = ultramafic rocks including carbonatites, lherzolites and pyroxenites.

those tuning parameters. Unlike PCA or K-means tests, which are unsupervised methods, SVM is a supervised statistical method, as the categorical information provided by the user is used to define the output and, additionally, the user defines the tuning parameters. SVM removes significant operator control of the classification process by eliminating visual inspection. In addition, it quantifies and records what control the operator retains, allowing full reproducibility. This is considered to be a highly desirable quality by the authors as bias and reproducibility issues caused by visual inspection of biplots can be eliminated. It should be noted that SVM is a binary classifier, and therefore grains are not individually assigned probabilities of belonging to one group or another by the classifier.

In the case of the bedrock dataset, SVM is carried out upon the coordinates of points on  $\text{Sr}/\text{Y}$  vs  $\Sigma\text{LREE}$  biplots (the most promising ratio and element-group abundances determined from PCA, e.g. Fig. 3b). To apply an SVM to the bedrock dataset equal numbers of training individuals per categorical class (so that no class is unduly weighted) are randomly sampled. The training individuals are then used to create a classification scheme, against which the grains that were not selected (test data) are plotted and the success rate determined. If the SVM can provide a satisfactory success rate for the grains of known composition, then unknown datapoints may be plotted.

PCA transformations, biplots, and SVMs were made using the "R" environment for statistical computing. Categorised PCA diagrams were made using the R library 'FactoMiner' (Lê et al., 2008). The code used to make the diagrams used in this paper, represents a combination of libraries (including e1071 for SVMs, Meyer et al., 2017; and ggplot2 for plotting graphics, Wickham, 2011) and code written by the authors, and is provided in a supplemental file.

## 4. Results

### 4.1. Discrimination of bedrock samples on the PCA and SVM biplots

Biplots are presented in Fig. 3 and the acronyms that will be used throughout the text are also restated there. The first biplot (Fig. 3a) is defined by the individual spot analyses from the bedrock apatite database, utilising the first two principal components from PCA of the bedrock apatite dataset. The utilised variables are La, Sr, Nd, Y, Lu, the Eu-anomaly (calculated from Sm, Eu and Gd according to the calculation of Shields and Stille, 2001), and a residual value ("CaPO")

representing unanalysed or non-utilised elements. Some bedrock data points had to be excluded from this PCA, as for example Y and Sr were not acquired in all of the bedrock apatite literature studies. Therefore, the authigenic category from the literature database is not used, though it is almost certainly a chemically distinct grouping as demonstrated on the multi-element spectra (Fig. 2).

The PCA biplot presented in Fig. 3a, and the radial diagram in Fig. 4 indicate that Sr and Y (and the HREEs, i.e. Lu) are anti-correlated (i.e. their trends are almost diametrically opposed), and that the LREEs (La and Ce) are anti-correlated to the residual representing "stoichiometric" apatite (i.e. trace-element poor apatite). Thus, although PCA biplots may be directly used to display unknown data, biplots of  $\text{Sr}/\text{Y}$  vs  $\Sigma\text{LREE}$  are used henceforth in this study (Fig. 3b). The data separation is comparable and the interpretation of datapoints on a  $\text{Sr}/\text{Y}$  vs  $\Sigma\text{LREE}$  biplot is much more intuitive to the geochemist than a biplot of 'PC1' vs 'PC2'. This methodology may also find a broader appeal than the PCA methodology due to its simpler implementation.  $\text{Sr}/\text{Y}$  ratios have previously been proposed as a useful discriminatory ratio in apatite (Belousova et al., 2002), but paired with a second axis of  $\Sigma\text{LREE}$  (and with the large dataset at our disposal) it is possible to delineate more bedrock fields with a higher confidence than was previously achievable, and to avoid co-plotting unrelated groups.

On a  $\text{Sr}/\text{Y}$  vs  $\Sigma\text{LREE}$  biplot (Fig. 3b) there are three broad trends that

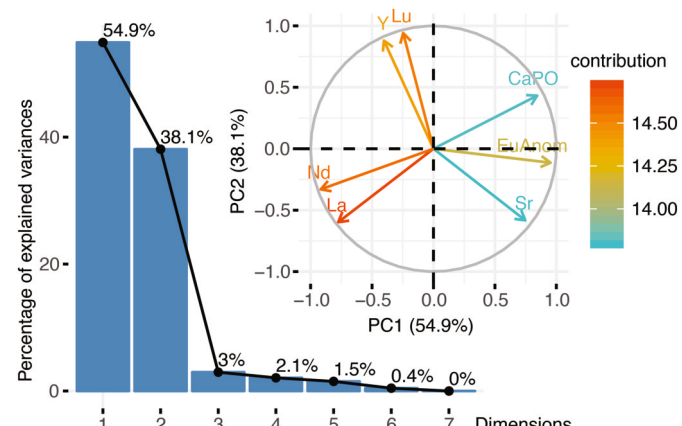


**Fig. 4.** Metadata for the PCA transformed data displayed in Fig. 3a.

should be noted. Firstly, increasing metamorphic grade, culminating in melting and anatexis, is associated with increasing LREE contents and a decrease in the Sr/Y ratio (note that this is caused both by increasing concentration of Y *and* by decreasing concentration of Sr, Table S1). Secondly, the Sr/Y ratio of igneous apatite is very indicative of the magma chemistry (as previously indicated by Belousova et al., 2002), with the exception of apatite from alkali-rich melts in which apatite is instead recognised by its extremely high LREE-contents as Sr/Y ratios are not diagnostic. Consequently, Sr/Y ratios cannot be used alone in apatite source type discrimination, as alkali-rich igneous grains and metamorphic grains in detritus would co-plot with all other igneous categories. Lastly, dissolution-reprecipitation of apatite during low-grade metamorphism will shift a given grain to the northwest quadrant on this biplot, as the REEs and Y are not typically reincorporated into low-grade metamorphic apatite upon reprecipitation (e.g. Harlov, 2011, 2015).

The SVM (Fig. 3c) is trained from the coordinates of the datapoints on biplot in Fig. 3b. Visual inspection shows the categorisation to be sensible and not over-fit. The tuning parameters used for the SVM are included in the “R” code provided with this paper. A matrix showing the SVM success rate (implemented according to the train/test split described in the methodology) over 32 iterations using different train/test splits is also provided (Fig. 5). The overall success rate of 85.2% per class (this number is derived as an arithmetic mean, simply the sum of the success rates of the classes divided by the number of classes; the maximum and minimum group success rates are 98% and 65%) is considered to be suitable to apply the classification to unknowns, especially given the multiclass SVM.

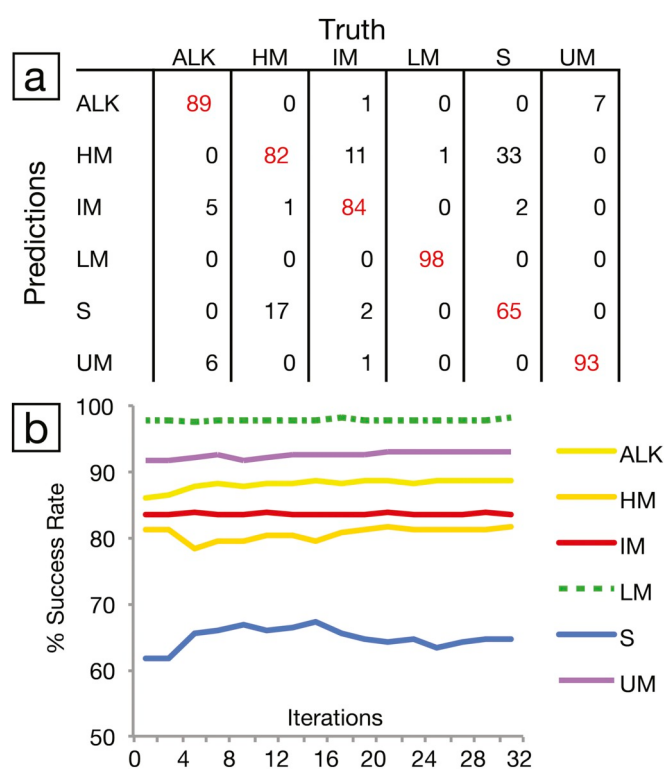


**Fig. 5.** (a) Success rate of the SVM classifier applied to the Sr/Y vs  $\Sigma$ LREE biplot on Fig. 3c averaged after 32 iterations and normalised to 100% per class. Note values are rounded and so may not add to exactly 100. Also note that incorrectly classified grains are from adjacent (partially overlapping) groups on a biplot and that share a similar petrogenesis (e.g. S and HM). The success rate of every class is well in excess of random chance given the 6-class SVM, which would be 16.67% per class. (b) Success rate of the SVM compared to number of iterations, the success rate of the SVM quickly plateaus meaning that few, or even a single iteration is acceptable for unknown characterisation.

The categorised data used for PCA and SVM are also presented on kernel density estimate diagrams of the input data (Fig. 6), including data for elements (U, Mn) and classes [AUT] that had to be cut as there were too few data points to use for a Support Vector Machine. These diagrams demonstrate that some of the non-utilised elements may be useful for category-separation once more bedrock data have been published using these elements.

#### 4.2. Apatite geochemistry applied to case study 1 – Mesoproterozoic sediments from NW Scotland

##### 4.2.1. Short background

Detrital apatite U–Pb age and trace-element data from the study of Kenny et al. (2019) are re-investigated here to assess whether more specific provenance interpretations can be made by comparison with the bedrock apatite database. The analysed apatite comes from the Stoer Group, a 2 km-thick continental and lacustrine Mesoproterozoic sedimentary sequence in NW Scotland that was deposited unconformably on TTG (Tonalite-Trondhjemite-Granodiorite)-dominated Archaean crystalline basement of the Lewisian Complex (Stewart, 2002). The Stoer Group is a pre-Grenvillian sequence deposited near the margin of the Laurentian supercontinent that avoided Grenvillian deformation, and has yielded impact-related authigenic feldspar  $^{40}\text{Ar}/^{39}\text{Ar}$  dates of  $1177 \pm 5$  Ma near the top of the sequence (Parnell et al., 2011), in an ejecta layer known as the Stac Fada Member (e.g., Simms, 2015). The section was sampled below, within and above the Stac Fada Member at both Gruinard Bay and the Bay of Stoer for U–Pb detrital zircon and apatite analyses.

Based on these U–Pb data, Kenny et al. (2019) found no significant change in apatite or zircon provenance below, within or above the Stac Fada Member, indicating that either: i) there was no large-scale drainage reorganisation after the Stac Fada impact event; ii) drainage-network reorganisation did take place following the bolide impact, but the configuration of the sediment source areas was such that it could not be detected using the detrital provenance methods employed; or iii) sediment reworking and/or aeolian sediment input (as documented in overlying units by Ielpi and Ghinasi, 2015) homogenised the detrital signal.

##### 4.2.2. Stac Fada apatite geochemistry results

The trace-element compositions of the dated apatite detritus in the Stoer Group sedimentary rocks are dominated by apatite of low- to medium-grade metamorphic (LM, 461 grains) affinity (cf. El Korb et al., 2009; Henrichs et al., 2018), with a subsidiary population of apatite with I-type granitoid to mafic igneous compositions (IM, 118 grains). 45 grains have high-grade metamorphic compositions (HM), while there are few apatite grains with compositions matching those of apatite from alkali-rich igneous rocks (ALK, 3 grains), ultramafic rocks (UM 22 grains), or S-type and felsic I-type granites (S, 3 grains) (Fig. 7).

When apatite U–Pb age data are considered along with their respective trace element compositions, there is a clear link between lithology and whether an apatite grain reveals an age within acceptable uncertainty (i.e. “dateable” grains with a  $^{207}\text{Pb}$ -corrected U–Pb age uncertainties of < 10%, Kenny et al., 2019). In particular, a greater proportion of low-grade metamorphic apatites than any other group are excluded (greyed-out points on Fig. 7). This is in agreement with studies of apatite from low- to medium-grade metamorphic bedrock which show that it is commonly extremely depleted in U and has low  $\text{Pb}^*/\text{Pb}_c$  ratios (e.g. Henrichs et al., 2018). The least dateable grains are those with both low LREE contents and very high Sr/Y ratios; in comparison LREE-poor grains with low Sr/Y are often possible to date (Fig. 7). Note that on that biplot the probability that detritus can be dated decreases towards the northwest quadrant. The divalent cations  $\text{Sr}^{2+}$  and  $\text{Pb}^{2+}$  have very similar ionic radii, whereas  $\text{U}^{4+}$  and  $\text{Y}^{3+}$  both have similar yet smaller ionic radii (Fig. 1). Low Sr/Y correlates with favourable  $\text{Pb}^*/\text{Pb}_c$  ratios that permit precise U–Pb dating in apatite. Overall, the

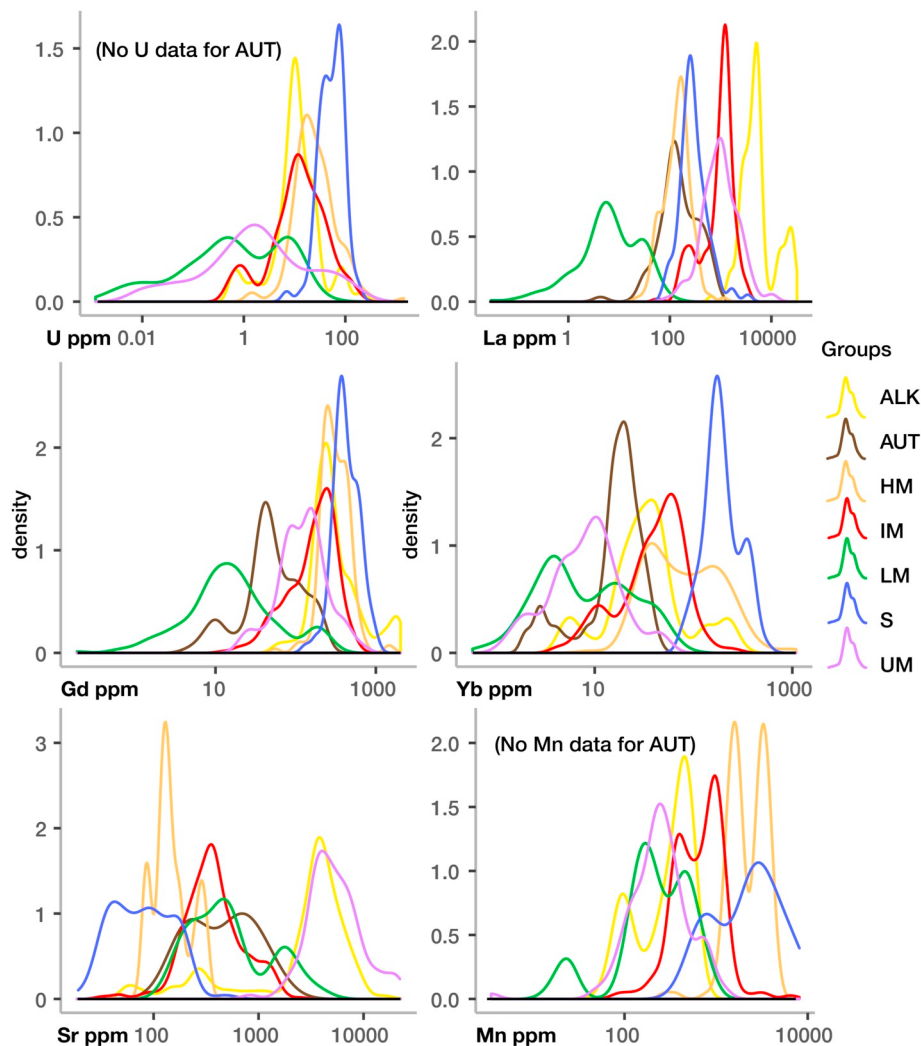


**Fig. 6.** Kernel Density Estimate (KDE) distributions of apatite trace element data (ppm) for individual elements from the compositional database, including elements (U and Mn) and a group (AUT) that are not implemented in the PCA-SVM methodology due to insufficient data density. Data are grouped according to the schemes described in Figure and 3.

proportion of non-dateable apatite grains is quite low in the Stoer Group sediments, and even the majority of LM detritus can be dated. This may be related to the fact that all apatite detritus is older than 1 Ga, as over long timescales even low-U apatite will accumulate appreciable radiogenic-Pb.

U–Pb grain ages of unknowns are displayed on a kernel density plot (KDP) in Fig. 8, and are broken down into three categories as defined by the SVM in Fig. 7; igneous (all igneous fields including S, ALK, IM and UM), high-grade metamorphic (HM), and low- to medium-grade metamorphic (LM). Zircon U–Pb ages from the same samples are also displayed. When divided by composition and plotted as separate KDEs, apatites with different chemistries characterise different events. Of most interest is the cluster of age peaks for all categories around 1.71–1.59 Ga. These correspond to the Laxfordian orogenic event, well represented in NW Scotland (e.g. Kinny et al., 2005). In this portion of the KDE plot there is a peak of igneous apatite ages at c. 1.71 Ga, followed by a peak in low- to medium-grade apatite ages at c. 1.65 Ga, and followed lastly by a gradually increasing signal of high-grade metamorphic apatite that culminates in a peak of apatite U–Pb ages at c. 1.59 Ga. We speculate that this sequence of ages may represent the accretion and metamorphism of an arc terrane (igneous age peak followed by low-grade metamorphic age peak), and its subsequent unroofing through time to reveal the high-grade orogenic core (high-grade metamorphic peak). Regardless of this speculation, these results

demonstrate a strong correlation between lithology and age in detrital apatite, with specific lithologies dominating particular time-intervals and thus tectonic events, and thus rendering it capable of distinguishing between sources. A 2.75 Ga peak that is not represented in the apatite record dominates the zircon U–Pb age record in the Stoer sediments. Zircon with ages younger than 2.75 Ga are uncommon, but they correlate most strongly with age-peaks characterised by igneous apatite (e.g. 2.5 Ga and 1.85 Ga). The Laxfordian event is poorly represented in the zircon U–Pb record even though most apatite in the Stoer Group yields Laxfordian U–Pb ages.

#### 4.3. Case study 2 – modern sediments, River Tarn, Central France

Case study 2 considers apatite from modern river sediment from the river Tarn in the southern Massif Central of France. These data are taken from O'Sullivan et al. (2018), where they were displayed on a PCA biplot based on bedrock apatite data from a smaller literature database than that used in this paper, and where unknown data were categorised using visual inspection. The Tarn and its tributaries drain the Cévennes sub-range of the Massif Central, which is composed of metasediments which experienced greenschist- to lower-amphibolite facies peak-Variscan metamorphism, and post-Variscan granitoids of broadly monzogranitic composition. A concise geological history of the southern Massif Central can be found in O'Sullivan et al., (2018), and in

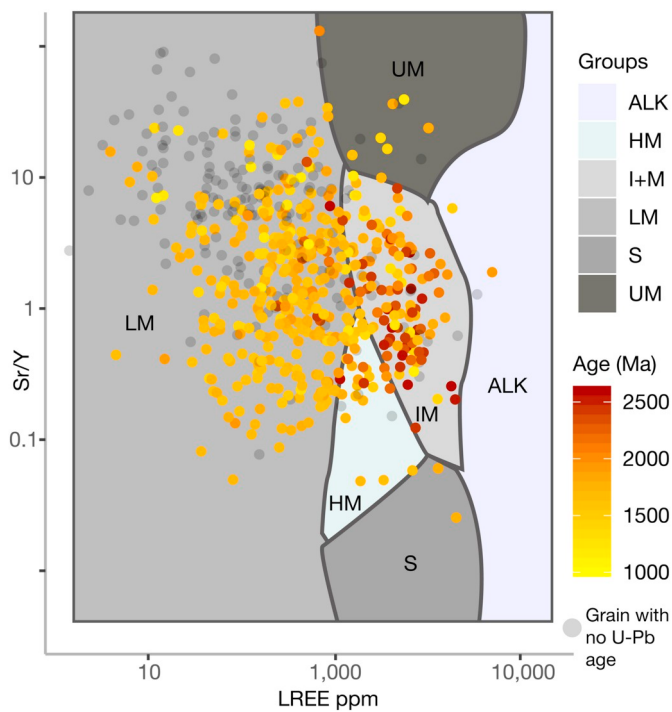


**Fig. 7.** Detritus coloured by age compared to the literature data SVM (same fields as in Fig. 3, but in greyscale to avoid confusion with unknown datapoints). Note that older detritus (brown) are more often igneous. Unknown datapoints filled in grey are grains that were considered not possible to date by Kenny et al., 2019. (For interpretation of the references to colour in this figure legend, the reader is referred to the web version of this article.)

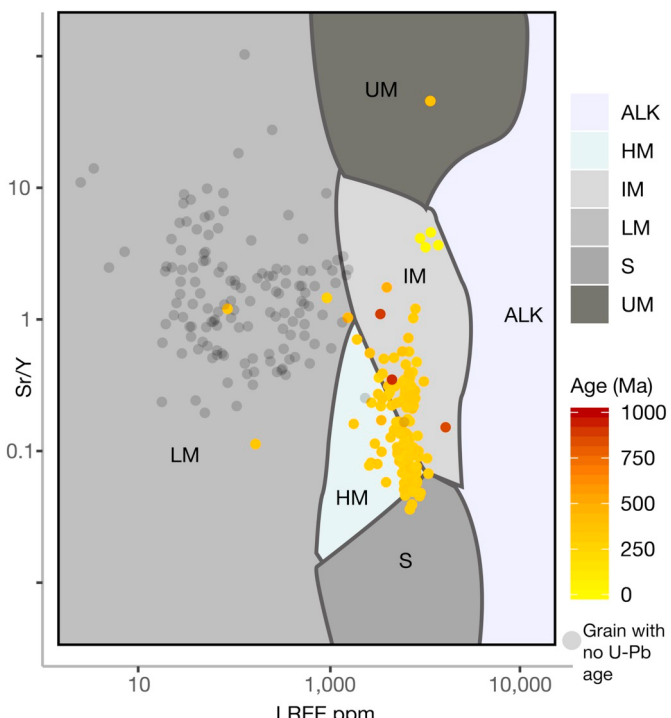


**Fig. 9.** Detrital apatite from the river Tarn plotted on Sr/Y vs  $\Sigma$ LREE SVM biplot and coloured by U–Pb age (undated grains in grey). Four different sediment provenances are clearly demonstrated: post-Variscan granitoids (c. 305 Ma orange points), metapelites (mostly not dated but traced upstream to low-grade Variscan graphitic schists), recent mafic volcanism (light yellow points) and pre-Variscan detritus of diverse protolith (brown points). Non-dateable grains were defined in O'Sullivan et al. (2018) as those having uncertainties larger than 20% on the  $^{207}\text{Pb}$ -corrected U–Pb age. Abbreviations the same as those defined in Fig. 3. (For interpretation of the references to colour in this figure legend, the reader is referred to the web version of this article.)

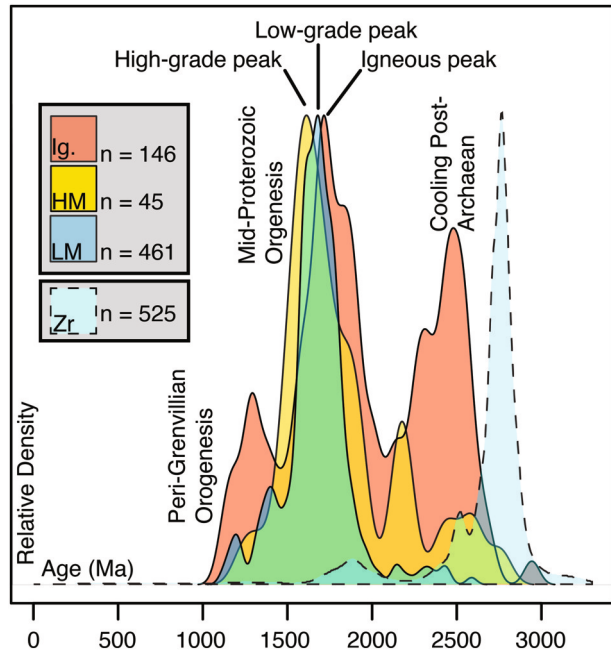


**Fig. 8.** KDE plot of detrital apatite and zircon U–Pb ages from the Stoer Group sedimentary rocks (U–Pb data from Kenny et al., 2019). Lithologies defined according to the SVM in Fig. 6; note that the 'R' code published with this paper (Supplementary file S3) provides a .txt file containing the SVM prediction for every individual input unknown data point. Igneous apatite is a combination of S, ALK, IM and UM. Graph created using the 'R' statistical environment.

more detail in Faure et al. (2009).

Detrital apatite from the Tarn and its tributaries show different

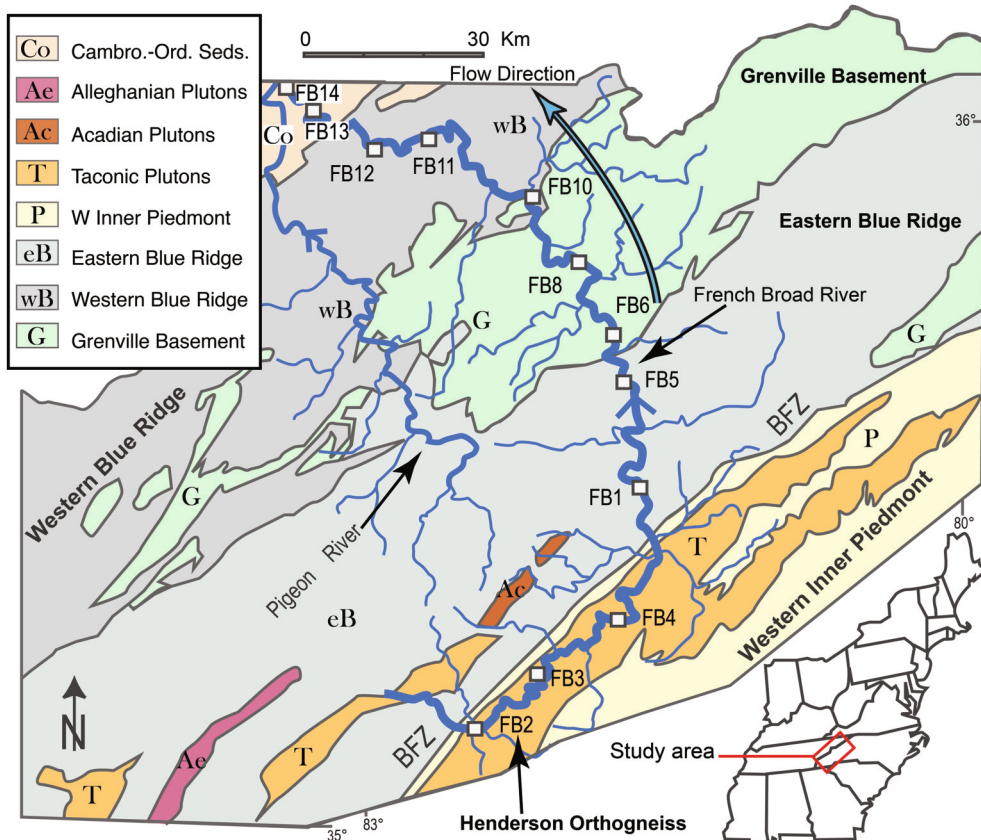
lithological affinities according to the sampled portion of the drainage system. A sample draining Variscan metamorphic rocks primarily yields apatite detritus that overlaps with low- to medium-grade metamorphic apatite from the literature (e.g. El Khorh et al., 2009; Henrichs et al., 2018), a sample draining the post-Variscan Cévennes granitoids is composed primarily of apatite with a strong geochemical affinity to granitoid apatite from the literature (e.g. Hsieh et al., 2008), while a sample draining an area containing a Miocene basanite pipe contains a very minor sub-population of apatite of mafic igneous trace-element affinity (e.g. Tang et al., 2012) and yielding Miocene U–Pb ages. Samples downstream of the mixing point of these streams show all three integrated trace-element and U–Pb age populations (and some pre-Variscan grains with older ages and diverse compositions), with clear separation on a Sr/Y vs  $\Sigma$ LREE biplot (Fig. 9). These results demonstrate a clear link between trace-element composition and both age and amenability to U–Pb dating; most igneous apatite yielding ages with acceptable uncertainties whilst LM apatite is almost entirely non-dateable.

#### 4.4. Case study 3 – modern sediments, French Broad River

##### 4.4.1. Background information

Case study 3 considers apatite in modern fluvial detritus from the French Broad River (FBR). Apatite trace-element data from the study of O'Sullivan et al. (2016) have been plotted on a PCA discriminant diagram to investigate whether new provenance information can be obtained, as the original study relied solely on the U–Pb ages of the detritus.

The FBR is an orogen-bisecting river in the southern Appalachians



of North Carolina and Tennessee in the United States (Fig. 10). The drainage basin of the FBR has been affected by three major phases of post-Grenville (c. 1 Ga) Appalachian orogenesis - the Taconic orogeny at c. 470–440 Ma, the Neoacadian orogeny at c. 370 Ma, and the Alleghanian orogeny at c. 320–290 Ma. U–Pb zircon and monazite (Hietpas et al., 2010) and U–Pb apatite and rutile (O'Sullivan et al., 2016) ages have all been published for the FBR detrital samples and all employ the original Hietpas et al. (2010) sample suite. The zircon U–Pb dataset fails to record the magma-poor Alleghanian (c. 320 Ma) orogeny, whereas monazite, rutile and apatite do. This is because these phases, unlike zircon, can grow during metamorphism, or if they are pre-metamorphic phases their U–Pb ages can be reset at medium- to high-metamorphic grades.

#### 4.4.2. Biplots and results

Two suites of samples from the French Broad River are presented on separate biplots in Fig. 11. The upstream samples (FB2, FB3 and FB4) are located within the outcrop of the Henderson gneiss within the Western Inner Piedmont (WIP) and adjacent to the Brevard Fault Zone (Fig. 10). The downstream samples (FB11, FB13 and FB14) were collected from the lower reaches of the FBR as it exits the Appalachians flowing to the west after draining the Western and Eastern Blue Ridge terranes (WBR and EBR), Grenvillian basement windows, and non-metamorphosed Upper Palaeozoic sediments of the Valley and Ridge province (Fig. 10).

In the upstream samples (Fig. 11a) the apatite detritus is largely characterised by a relatively simple assemblage of low- to medium-grade metamorphic apatite (LM), and plentiful high-grade metamorphic apatite (HM), with a very small population of igneous grains. The U–Pb ages are not particularly dispersed, with most detrital apatite U–Pb ages ranging between c. 290–400 Ma, and thus within age uncertainty of the Alleghanian (~ 320 Ma) and Neoacadian (~ 370 Ma) orogens.

**Fig. 10.** Map of sample locations and terranes within the FBR catchment, modified from O'Sullivan et al. (2016). Detrital samples FB2, FB3 and FB4 are taken from the FBR within the Henderson orthogneiss of the Western Inner Piedmont Terrane and source rocks that have experienced high metamorphic grades; the downstream samples FB11, FB13 and FB14 integrate detritus from a much wider range of lithologies and metamorphic grades. The Blue Ridge terranes are predominantly composed of polymetamorphosed metasedimentary rocks. (For interpretation of the references to colour in this figure legend, the reader is referred to the web version of this article.)

In the downstream samples (Fig. 10, FB11; FB13; FB14), the age and trace-element signal is more dispersed (Fig. 11b) as sediment has been sourced from a much larger catchment area (Fig. 10). In these samples Grenvillian-age apatite detritus with igneous compositions is now present (Fig. 11b). These grains can thus be linked to source areas that have not experienced Appalachian tectonothermal events. The proportion of apatite with high-grade metamorphic compositions and Neoacadian-Alleghanian ages, a common sediment component in the upstream segment of the main river channel, has now been substantially diluted downstream (to just 12 of the 120 grains that yielded U–Pb ages in the downstream samples vs 55 of the 135 successfully U–Pb dated grains upstream). The proportion of grains with LM compositions is, contrastingly, significantly higher downstream as the FBR drains westwards towards the external domain of the Appalachian orogen (Fig. 10).

## 5. Discussion

### 5.1. Provenance determinations using the apatite database

On the bedrock discriminant biplots and SVM (Fig. 3), the apatite trace-element data are separately plotted into six broad lithological classes: 1) high-grade metamorphic, leucosome and anatexitic rocks (HM); 2) felsic granitoids (S); 3) mafic granitoids-to-mafic igneous rocks (IM); 4) syenites and other alkali-rich igneous rocks (ALK); 5) ultramafic igneous rocks (UM); 6) low- and medium-grade metamorphic and metasomatised rocks (LM). These data show that apatite trace-element compositions can be convincingly related to their source-rock lithology, and additionally, that apatite trace-element data from multiple studies are consistent with each other in terms of their trace-element systematics. Hence, the geochemical heterogeneity of natural apatite and the high quality and large volume of the available published data means that apatite can be used to determine its source protolith in

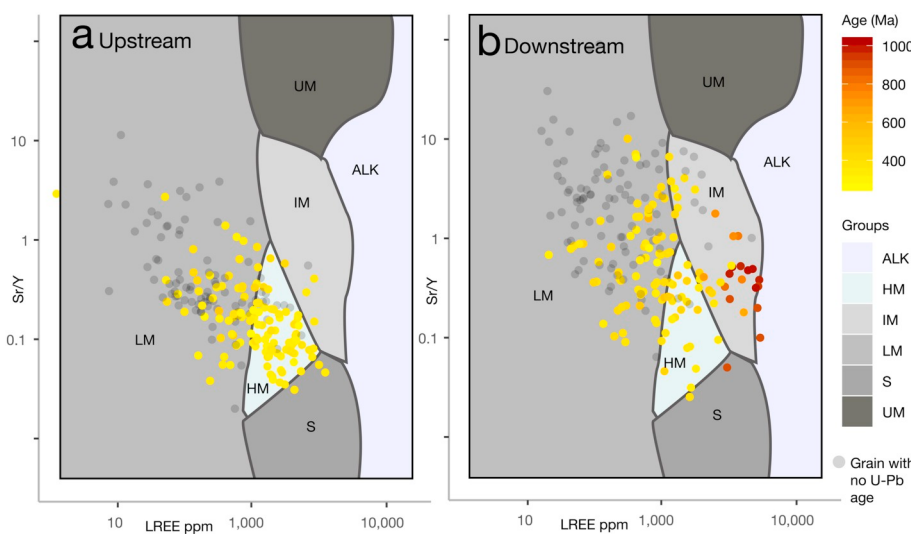


**Fig. 11.** Comparison of detrital apatite compositions and U–Pb ages in (a) upstream samples (FB2, FB3 and FB4, Fig. 10), and (b) downstream samples (FB11, FB13 and FB14, Fig. 10). Data are displayed on Sr/Y vs  $\Sigma$ LREE biplots with overlaid SVM category boundaries. Unknown data points coloured grey were those considered not possible to date by O'Sullivan et al. (2016).

sedimentary detritus or volcaniclastic rocks, with a margin of error that varies by lithological category, with the greatest uncertainty at the felsic igneous [S] and high grade metamorphic [HM] boundary, and least uncertainty associated with the ultramafic igneous [UM], alkali-rich igneous [ALK] and low- and medium-grade metamorphic [LM] categories.

While apatite trace-element compositions have previously been used successfully as a provenance indicator (e.g. Abdullin et al., 2016; Dill, 1994; Malúsa et al., 2017; Morton and Yaxley, 2007; O'Sullivan et al., 2018) and to track ash-fall deposits (e.g. Sell et al., 2015), and Sm–Nd isotopic compositions (e.g. Carter and Foster, 2009) have also been used to track apatite provenance, the data synthesis in this paper provides a simple, repeatable recipe for apatite discrimination that synthesises a more diverse range of bedrock lithologies than has been implemented before. Only six elements with low analytical backgrounds on LA-ICP-MS and high concentrations in apatite (La; Ce; Pr; Nd; Y and Sr) are required to determine the source rock composition; adding these six trace elements to an LA-Q-ICP-MS U–Pb apatite dating session will not significantly compromise the quality of U–Pb age data, as they can be determined with sufficient precision using short (10 ms or less) dwell times.

The SVM methodology employed in this paper is capable of classifying unknowns based on the classification used for the bedrock ‘knowns’ with an overall average success rate per class of c. 85% (Fig. 5). While this means that c. 15% of bedrock data points per class are incorrectly categorised (varying from 2% misclassified ‘LM’ data points, to 35% of ‘S’ data points, Fig. 5), the success rate is considered high enough to be useful for provenance studies, especially considering that the failure rate given random chance for a classification scheme with six classes would be c. 85% per class. An advantage of the SVM methodology applied to geochemical data is that it permits full reproducibility. SVM does not eliminate bias, as it is based upon samples, categories and tuning parameters selected by the user. But it offers the advantage that these biases can be recorded and reproduced given the same samples, categories and tuning parameters, thus facilitating rapid comparison of datasets of unknowns from different authors and studies. The regions with the highest failure rate of the SVM classifier are near the IM/HM and S/HM category boundaries (Fig. 3c). Thus, incorrectly classified grains are predominantly split between one of two closely related categories (i.e. HM or IM; HM or S, Fig. 5) amongst six in total. As the HM category includes granulites and partial-melts it is not surprising that the chemical composition of apatite in these rocks is sometimes very similar to that of granitoids in the IM and S fields, which may in some cases comprise melts that are geochemically indistinguishable from melanosome or leucosome material respectively. It

is unsurprising that a categorical system imposed on such data should not provide complete class separation, as categorisation of such rocks is an artificial construct imposed upon rocks existing along a continuum of compositions. Demonstrating this, the categories that plot away from the high-grade metamorphic field have much higher success rates (e.g. LM and UM bedrock apatite are misclassified c. 5% of the time Fig. 5).

Selected elemental concentrations of the different apatite categories are presented on kernel density estimate (KDE) diagrams in Fig. 6. These KDEs include data for elements (U and Mn) and groups (AUT – authigenic) not used in the SVM for reasons explained in the methods section, and indicate that other trace elements may be useful for apatite categorisation once more data are published. As the concentration of U in apatite is an important factor governing the precision with which apatite may be dated, this diagram also hints at the biases that may affect apatite age datasets, as apatite from low-grade metamorphic and ultramafic igneous rocks mostly have considerably lower U abundances than apatite from high-grade metamorphic and non-ultramafic igneous rocks, meaning that apatite from certain categories are less likely to be successfully dated than apatite from other categories.

The methodology developed in this paper also negates the need to undertake bedrock sampling of potential source areas, as apatite trace element composition data for similar lithologies collected by different authors in different locations are demonstrated to be consistent (Fig. 3). This means that the method can be applied to ancient detritus whose source-areas are non-extant, though of course sensu stricto the source rock of *any* detritus is by *definition* non-extant.

Ultimately, SVM is simply a tool that we have used to aid reproducibility in unknown categorisation, the results of which should not be taken solely at face value. A geologist should take note of discrepancies in the categorical output of the SVM from what they expect, and override those outputs should they have sound reasoning to suspect that those outputs are incorrect. Extra consideration should be given to points lying on the HM/S boundary. This is especially true as the SVM is wholly dependent upon a comprehensive bedrock apatite dataset but whose categorisation scheme we have chosen, and that nevertheless may still not fully constrain certain litho-categorical boundaries.

## 5.2. Discussions of case studies: practical geological implications of the method

As the methodology developed in this paper has been applied to real-world examples, the subject of provenance using apatite composition warrants significant discussion, as do the implications for datasets integrating U–Pb age data and trace element geochemistry in apatite.

Due to the limited variety and simple arrangement of lithologies in the upper river Tarn catchment, the river Tarn study provides the clearest separation of detrital apatite populations in the case studies discussed in this paper, and provides a good starting point for this discussion. The simple distribution of non-deformed post-Variscan granitoids, peak-Variscan metamorphic rocks, and recent mafic volcanism (e.g. Brichau et al., 2008; Faure et al., 2009) leads to a trimodal distribution of apatite compositions on biplot (Fig. 9), and demonstrates the faithfulness of apatite trace element composition to the lithology it is derived from.

The link between lithology and amenability to U–Pb dating is also most evident in this case study. While a greater proportion of grains with igneous trace-element compositions are dateable than those with LM (low- to medium-grade metamorphic) compositions in every case study presented in this paper, this relationship is clearest in the river Tarn detrital samples as almost no grains with LM compositions were dateable. This may be due to the specific grade or protoliths of the metamorphic rocks in the river Tarn catchment, which are mostly greenschist-facies graphitic metapelites (Faure et al., 2009). Detrital rutiles derived from the metapelites in the Tarn catchment are also generally U-poor and Pb-rich (O'Sullivan et al., 2018).

Apatite in the Scottish case study, the Stoer Group sediments in proximity to the Stac Fada ejecta layer, do not display significant inter-sample apatite U–Pb or trace element variation, and thus do not record impact-related drainage reorganisation (Kenny et al., 2019). However, the intra-sample history recorded by the Stoer Group apatite is intriguing, and reveals tantalising details about the sequencing of orogenic events recorded by apatite detritus in this sediment. Of particular interest are the series of three age peaks that are each recorded by apatite of different composition in the period 1.71–1.55 Ga (Fig. 8). It is very simple to explain this succession of detrital apatite age-peaks as a result of the accretion of an arc-terrane to the Laurentian margin, and indeed these age-peaks correlate with the known ages of Laxfordian deformation in NW Scotland (e.g. Kiny et al., 2005). This event would be expressed as arc-magmatism (the oldest peak of the three, represented by an igneous (IM + S + UM + ALK) apatite U–Pb age peak, and also detected in the detrital zircon U–Pb record from the same samples; Kenny et al., 2019), followed by accretion and collisional metamorphism (LM and HM apatite U–Pb age peaks). Shallower metamorphic rocks will be exhumed above the apatite Pb-retention zone first or may have formed at low temperatures and thus reflect crystallization ages (LM age peak), thus the HM apatite U–Pb age-peak is the youngest as these apatites are recording exhumation from greater depth as the orogen is progressively denuded and/or the crust is extended post-collision.

The ability to de-convolute apatite age-composition populations made possible using the methodology described in this paper, has potential to unravel the history of cryptic orogenic events in highly deformed terranes such as NW Scotland. Apatite U–Pb age-peak deconvolution by lithology also produces narrower peaks (i.e. shorter in duration) than those that results from plotting all apatite age data on a U–Pb KDE simultaneously (cf. Kenny et al., 2019 with this work). Often, detrital apatite U–Pb age peaks are much broader than those obtained from the same samples by U–Pb zircon dating (e.g. O'Sullivan et al., 2016). While some of this effect is naturally due to the greater precision afforded by individual detrital zircon ages compared to those obtainable from a typical detrital apatite U–Pb analysis, some of this effect is also doubtless due to the greater range of lithologies that apatite crystallises in. The detrital zircon U–Pb record will mostly record only tectonic phases characterised by significant felsic plutonism (e.g. Hietpas et al., 2010; O'Sullivan et al., 2016); apatite will in comparison record all phases of orogenesis as it is variably crystallised, consumed, re-precipitated and age-reset throughout the duration of an orogenic cycle. The ability to de-convolute apatite by composition thus permits the detection of detritus derived from these different processes separately.

The French Broad River (FBR) case study demonstrates the faithfulness of apatite composition to the terrane or portion of an orogen it is derived from. The proportion of apatite from high-grade vs lower-grade metamorphic rocks changes according to position within the orogen in agreement with the regional metamorphic grade; just as the river Tarn case study demonstrated the fidelity of detrital apatite to the lithology it is derived from. In the upstream FBR samples (FB2, FB3, FB4, Fig. 10) the ages and compositions of apatite are more homogeneous than in the downstream samples (FB11, FB13, FB14, Fig. 10). Almost all dateable apatite grains in the upstream sample suite yield Acadian and Alleghanian U–Pb ages and a significant proportion are high-grade metamorphic (HM) in composition (55 of the 134 grains with Neoacadian-Alleghanian U–Pb ages, Fig. 11a and b). The lack of significant igneous apatite detritus with U–Pb ages consistent with Appalachian orogenesis in these samples indicates that all plutons emplaced into what is now the upper catchment of the FBR (e.g. the Taconic Henderson orthogneiss Fig. 10) have been pervasively overprinted both with respect to their apatite trace element geochemistry and U–Pb isotope systematics during the Neoacadian and/or Alleghanian orogenies.

In the downstream samples apatite has been sourced from a broader array of terranes, as herein the FBR has traversed the entire Appalachian orogen. In these samples there is much more apatite with IM and LM compositions than in the upstream samples (Fig. 11c and d). In particular there is a distinct population of Grenville-age detritus with trace element compositions matching those of bedrocks from the IM and S groups that is absent upstream (Fig. 11d). The appearance of much greater proportions of LM detritus and pristine Grenvillian apatite with igneous compositions is consistent with the sampling locations of these detrital samples; i.e. west of the main regions affected by higher-grade metamorphism in the external portion of the Appalachian orogen (Fig. 10).

While there are only a limited number of Grenville-age grains in the studied samples, almost all (17/18) have igneous compositions. This contrasts with 22/219 (10%) igneous grains in the dateable Appalachian-age detritus (grains with U–Pb ages under 460 Ma aggregated from all six samples). This highlights stark differences in the dominant apatite populations in the Grenville and Appalachian orogens in this region. It can also help to explain the paucity of detrital Neoacadian and Alleghanian zircon U–Pb ages in the FBR, as detrital zircon U–Pb is a poor recorder of sub-anatetic metamorphism (e.g. Hietpas et al., 2010; O'Sullivan et al., 2016). In comparison the trace-element composition of detrital apatite from the Appalachian orogen is almost entirely metamorphic (LM and HM) and thus consistent with the magma-poor character of the Neoacadian and Alleghanian orogenies in the southern Appalachians (O'Sullivan et al., 2016).

In common with the Stac Fada case study from NW Scotland, apatites with LM trace-element compositions are sometimes dateable in the FBR; and indeed due to the large volume of LM apatite in this detritus they comprise the majority of dated grains in both studies. This is in stark contrast with the river Tarn (Massif Central) case study, wherein LM detritus is almost entirely non-dateable. This begs the question what are the differences between apatite detritus with LM compositions from the Southern Appalachians and the Lewisian of Scotland on one hand, and the southern Massif Central on the other?

The river Tarn mainly sources pelitic schists that have experienced single-phase peak-Variscan low to medium-grade metamorphism, whereas the FBR and Stoer Group are at least partly derived from polyphase high-grade metamorphic basement with diverse protolith types including igneous protoliths, with variable low-grade overprinting. This indicates that it is potentially not just metamorphic grade, but also protolith type that determines whether metamorphic apatite is amenable to U–Pb dating. Additionally, perhaps polyphase metamorphism (which occurred in the sources of the FBR and Stac Fada samples, but not in the Cévennes) makes apatite more amenable to U–Pb dating, as apatite in high-grade metamorphic rocks might not necessarily re-precipitate (and therefore release U to other phases)

during subsequent lower-grade events due to being armoured within dehydrated assemblages and thus protected from fluid interaction (similar to the behaviour documented for rutile from such lithologies (e.g. Luizotto et al., 2009). Those few older apatite grains (i.e. pre-Variscan) present in the Tarn/Cévennes detritus are diverse in both age and composition, indicating that they are likely present as a detrital component in the Cévennes metapelites. This could putatively be due to shielding within unreactive lithologies during metamorphism, though another origin for these grains is also possible.

## 6. Conclusions

- The literature synthesis presented in this paper, combined with the statistical approach (PCA and SVM) applied to our collated literature dataset, demonstrates that apatite-trace element geochemistry is consistently and systematically diverse. Using this methodology a Sr/Y vs  $\Sigma$ LREE biplot is found to be a simple tool that can discriminate the broad provenance of apatite from essentially all common lithologies.
- Six broad categories of apatite are consistently identified in this dataset with various degrees of overlap: low- and medium-grade metamorphic apatite; high-grade metamorphic apatite; felsic granitoids; mafic granitoids and mafic igneous apatite; alkali-rich igneous apatite and ultramafic-carbonatitic apatite.
- As more bedrock data on apatite trace elements are published in the future, it will be possible to discriminate additional categories of apatite and to refine categorical boundaries. For example, authigenic apatite is clearly chemically distinct ([AUT] on Fig. 2), but is not sufficiently well characterised to be used in our methodology. Furthermore, “mafic granitoids and mafic igneous apatite” [IM] is a relatively broad group and additional data may help to subdivide this category. Finally, while Sr/Y vs  $\Sigma$ LREE biplots are a very useful tool to discriminate broad apatite provenance, there may be scope to use other element ratios to determine very specific provenances within the six categories discussed here.
- Coupled with its utility as a chronometer, the methodology developed here means that detrital apatite can thus provide specific provenance information to fingerprint likely source rock(s), including mafic igneous lithologies that typically contribute little zircon to detritus. The statistical approach taken in this paper also has potential to be applied to other detrital minerals, including zircon.
- As a minimum of only five REYs and Sr are required as discriminant elements in the biplots presented in study, the analytical protocol needed to reproduce the provenance methodology in this paper can be readily and cost-effectively replicated, and can easily be included alongside U–Pb isotope analysis in a single LA-Q-ICP-MS analytical protocol.
- Using detrital apatite trace element compositions, it is possible to de-convolute detrital apatite U–Pb age data by lithology. This permits the identification of sub-events within orogenic cycles in detritus that are otherwise masked or smoothed over by plotting all apatite U–Pb age data together.
- Apatite U contents vary consistently by lithological category. Ultramafic igneous and low- and medium-grade metamorphic apatite have low U abundances while all other categories contain significantly more U. Apatite age-only datasets will thus be biased against ultramafic rocks and greenschist/amphibolite-facies rocks.
- The methodology developed in this paper has potential application as a REE-placer vectoring tool, particularly as apatite from melts with carbonatitic or alkali-rich igneous compositions may reliably be discerned.
- The methodology developed here also has potential as a tracer of skarn, porphyry or intrusion-related deposits. As the REYs are highly conservative in apatite in the absence of fluid-mediated reprecipitation, apatite will thus retain its igneous composition unless

metasomatised. Detrital apatite with low-grade/metasomatic compositions derived from igneous terranes may thus be useful detrital vectors of those deposit styles.

## Data availability

Supplementary data and code necessary to reproduce the SVM biplots used in this paper are included as supplemental files (S1 – S4) and are also available at the following link on pangaea.de: <https://doi.pangaea.de/10.1594/PANGAEA.906570>

## Declaration of Competing Interest

The authors declare that they have no known competing financial interests or personal relationships that could have appeared to influence the work reported in this paper.

## Acknowledgements

This material is based upon works supported by Science Foundation Ireland under grant 12/IP/1663. We would also like to thank Cora McKenna for her assistance during LA-ICP-MS data acquisition and Chris Mark for many fruitful discussions. This publication has also emanated from research supported in part by a research grant from Science Foundation Ireland (SFI) under Grant Number 13/RC/2092 and co-funded under the European Regional Development Fund and by PIPCO RSG and its member companies.

## Appendix A. Supplementary data

Supplementary data to this article can be found online at <https://doi.org/10.1016/j.earscirev.2019.103044>.

## References

- Resentini, A., Malusà, M.G., 2012. Sediment budgets by detrital apatite fission-track dating (Rivers Dora Baltea and Arc, Western Alps). *Geol. Soc. Am. Spec. Pap.* 487, 125–140.
- Abdullin, F., Solé, J., Solari, L., Shchepetilnikova, V., Meneses-Rocha, J.J., Pavlinova, N., Rodríguez-Trejo, A., 2016. Single-grain apatite geochemistry of Permian-Triassic granitoids and Mesozoic and Eocene sandstones from Chiapas, southeast Mexico: Implications for sediment provenance. *Int. Geol. Rev.* 58 (9), 1132–1157. <https://doi.org/10.1080/00206814.2016.1150212>.
- Aitchinson, J., 1982. The statistical analysis of compositional data (with discussion). *J. R. Statist. Soc. B* 44, 139–177.
- Ansquerque, C., Mark, C., Caulfield, J.T., Chew, D.M., 2019. Combined in-situ determination of halogen (F, Cl) content in igneous and detrital apatite by SEM-EDS and LA-Q-ICPMs: a potential new provenance tool. *Chem. Geol.* 524, 406–420. <https://doi.org/10.1016/j.chemgeo.2019.07.012>.
- Barbarand, J., Carter, A., Wood, I., Hurford, T., 2003. Compositional and structural control of fission-track annealing in apatite. *Chem. Geol.* 198 (1–2), 107–137. [https://doi.org/10.1016/S0009-2541\(02\)00424-2](https://doi.org/10.1016/S0009-2541(02)00424-2).
- Bea, F., Montero, P., 1999. Behavior of accessory phases and redistribution of Zr, REE, Y, Th, and U during metamorphism and partial melting of metapelites in the lower crust: an example from the Kinzigite Formation of Ivrea-Verbano, NW Italy. *Geochim. Cosmochim. Acta* 63 (7), 1133–1153. [https://doi.org/10.1016/S0016-7037\(98\)00292-0](https://doi.org/10.1016/S0016-7037(98)00292-0).
- Bea, F., Pereira, M.D., Stroh, A., 1994. Mineral/leucosome trace-element partitioning in a peraluminous migmatite (a laser ablation-ICP-MS study). *Chem. Geol.* 117 (1–4), 291–312. [https://doi.org/10.1016/0009-2541\(94\)90133-3](https://doi.org/10.1016/0009-2541(94)90133-3).
- Belousova, E.A., Walters, S., Griffin, W.L., O'Reilly, S.Y., 2001. Trace-element signatures of apatites in granitoids from the Mt Isa Inlier, Northwestern Queensland. *Aust. J. Earth Sci.* 48 (AUGUST), 603–619. <https://doi.org/10.1046/j.1440-0952.2001.00879.x>.
- Belousova, E.A., Griffin, W.L., O'Reilly, S.Y., Fisher, N.I., 2002a. Apatite as an indicator mineral for mineral exploration: Trace-element compositions and their relationship to host rock type. *J. Geochem. Explor.* 76 (1), 45–69. [https://doi.org/10.1016/S0375-6742\(02\)00204-2](https://doi.org/10.1016/S0375-6742(02)00204-2).
- Belousova, E.A., Griffin, W.L., O'Reilly, S.Y., Fisher, N.I., 2002b. Igneous zircon: trace element composition as an indicator of source rock type. *Contrib. Mineral. Petro.* 143 (2002), 602–622. <https://doi.org/10.1007/s00410-002-0364-7>.
- Bernoulli, D., Winkler, W., 1990. Heavy mineral assemblages from Upper cretaceous South- and Austroalpine flysch sequences (Northern Italy and Southern Switzerland): source terranes and palaeotectonic implications. *Eclogae Geol. Helv.* 83 (2), 287–310. <https://doi.org/10.5169/seals-166588>.

- Bingen, B., Demaiffe, D., Hertogen, J., 1996. Redistribution of rare earth elements, thorium, and uranium over accessory minerals in the course of amphibolite to granulite facies metamorphism: the role of apatite and monazite in orthogneisses from southwestern Norway. *Geochim. Cosmochim. Acta* 60 (8), 1341–1354. [https://doi.org/10.1016/0016-7037\(96\)00006-3](https://doi.org/10.1016/0016-7037(96)00006-3).
- Bouch, J.E., Hole, M.J., Trewin, N.H., Chenery, S., Morton, A.C., 2002. Authigenic apatite in a fluvial sandstone sequence: evidence for rare-earth element mobility during diagenesis and a tool for diagenetic correlation. *J. Sediment. Res.* 72 (1), 59–67. <https://doi.org/10.1306/040301720059>.
- Boyce, J.W., Tomlinson, S.M., McCubbin, F.M., Greenwood, J.P., Treiman, A.H., 2014. The Lunar Apatite Paradox. *Science* 344 (6182), 400–402. <https://doi.org/10.1126/science.1250398>.
- Brichau, S., Respaut, J.P., Monié, P., 2008. New age constraints on emplacement of the Cévenol granitoids, South French Massif Central. *Int. J. Earth Sci.* 97 (4), 725–738. <https://doi.org/10.1007/s00531-007-0187-x>.
- Broska, I., Williams, C.T., Uher, P., Konečný, P., Leichmann, J., 2004. The geochemistry of phosphorus in different granite suites of the Western Carpathians, Slovakia: the role of apatite and P-bearing feldspar. *Chem. Geol.* 205 (1–2), 1–15. <https://doi.org/10.1016/j.chemgeo.2003.09.004>.
- Bruand, E., Storey, C., Fowler, M., 2016. An apatite for progress: inclusions in zircon and titanite constrain petrogenesis and provenance. *Geology* 44, 91–94. <https://doi.org/10.1130/G37301.1>.
- Bruand, E., Fowler, M., Storey, C., Darling, J., 2017. Apatite trace element and isotope applications to petrogenesis and provenance. *Am. Mineral.* 102, 75–84. <https://doi.org/10.2138/am-2017-5744>.
- Carey, A., Samson, S., Sell, B., 2009. Utility and limitations of apatite phenocryst chemistry for continent-scale correlation of Ordovician K-bentonites. *J. Geol.* 117 (1), 1–14. <https://doi.org/10.1086/594368>.
- Carrappa, B., DeCelles, P.G., Reiners, P.W., Gehrels, G.E., Sudo, M., 2009. Apatite triple dating and white mica 40Ar/39Ar thermochronology of syntectonic detritus in the Central Andes: a multiphase tectonothermal history. *Geology* 37 (5), 407–410. <https://doi.org/10.1130/G25698A.1>.
- Carter, A., Foster, G., 2009. Improving constraints on apatite provenance: Nd measurement on FT dated grains. *Geol. Soc. Spec. Publ.* 324, 1–16.
- Chakhmouradian, A.R., Reguir, E.P., Zaitsev, A.N., Couëslan, C., Xu, C., Kynický, J., Mumtin, A.H., Yang, P., 2017. Apatite in carbonatitic rocks: Compositional variation, zoning, element partitioning and petrogenetic significance. *Lithos* 274–275, 188–213. <https://doi.org/10.1016/j.lithos.2016.12.037>.
- Chang, L.L.Y., Howie, R.A., Zussman, J., 1998. Rock-Forming Minerals, Vol 5b: Non-silicates: Sulphates, Carbonates, Phosphates and Halides, 2nd edition. The Geological Society, London, pp. 383.
- Cherniak, D.J., 2010. Diffusion in Accessory Minerals: Zircon, Titanite, Apatite, Monazite and Xenotime. *Rev. Mineral. Geochem.* 72 (1), 827–869. <https://doi.org/10.2138/rmg.2010.72.18>.
- Chew, D.M., Domelick, R.A., 2012. Combined apatite fission track and U-Pb dating by LA-ICP-MS and its application in apatite provenance analysis. In: Quantitative Mineralogy and Microanalysis of Sediments and Sedimentary Rocks. 42. Mineralogical Association of Canada Short Course, pp. 219–247.
- Chew, D.M., Petrus, J.A., Kamber, B.S., 2014. U-Pb LA-ICPMS dating using accessory mineral standards with variable common Pb. *Chem. Geol.* 363, 185–199. <https://doi.org/10.1016/j.chemgeo.2013.11.006>. Elsevier B.V.
- Chu, M.-F., Wang, K.-L., Griffin, W.L., Chung, S.-L., O'Reilly, S.Y., Pearson, N.J., Iizuka, Y., 2009. Apatite Composition: Tracing Petrogenetic Processes in Transhimalayan Granitoids. *J. Petrol.* 50 (10), 1829–1855. <https://doi.org/10.1093/petrology/egp054>.
- Clementi, E., Raimond, D.L., Reinhardt, W.P., 1967. Atomic screening constants from SCF functions. II. Atoms with 37 to 86 electrons. *J. Chem. Phys.* 47 (4), 1300–1307. <https://doi.org/10.1063/1.1712084>.
- Cogné, N., Chew, D., Stuart, F.M., 2014. The thermal history of the western Irish onshore. *J. Geol. Soc. Lond.* 171, 779–792. <https://doi.org/10.1144/jgs2014-026>.
- Danišák, M., 2019. Integration of fission-track thermochronology with other geochronologic methods on single crystals. In: Fission-Track Thermochronology and its Application to Geology. Springer, Cham, pp. 93–108.
- Dill, H.G., 1994. Can REE patterns and U-Th variations be used as a tool to determine the origin of apatite in clastic rocks? *Sediment. Geol.* 92 (3–4), 175–196. [https://doi.org/10.1016/0037-0738\(94\)90105-8](https://doi.org/10.1016/0037-0738(94)90105-8).
- Dill, H.G., Weber, B., Klosa, D., 2012. Morphology and mineral chemistry of monazite-zircon-bearing stream sediments of continental placer deposits (SE Germany): Ore guide and provenance marker. *J. Geochem. Explor.* 112, 322–346. <https://doi.org/10.1016/j.gexplo.2011.10.006>.
- Dodson, M.H., 1973. Closure temperature in cooling geochronological and petrological systems. *Contrib. Mineral. Petrol.* 40 (3), 259–274. <https://doi.org/10.1007/BF00373790>.
- Ehlers, T.A., Farley, K.A., 2003. Apatite (U-Th)/He thermochronometry: methods and applications to problems in tectonic and surface processes. *Earth Planet. Sci. Lett.* 206 (1–2), 1–14. [https://doi.org/10.1016/S0012-821X\(02\)01069-5](https://doi.org/10.1016/S0012-821X(02)01069-5).
- El Khor, A., Schmidt, S.T., Ulianov, a, Potel, S., 2009. Trace element partitioning in high-pressure metamorphic assemblages during subduction-related metamorphism, Ille de Groix, France: a Detailed LA-ICPMS Study. *J. Petrol.* 50 (6), 1107–1148. <https://doi.org/10.1093/petrology/egp034>.
- Emerson, N., Simo, J., Byers, C., Fournelle, J., 2004. Correlation of (Ordovician, Mohawkian) K-bentonites in the upper Mississippi valley using apatite chemistry: implications for stratigraphic interpretation of the mixed carbonate-siliciclastic Decorah Formation. *Palaeogeogr. Palaeoclimatol. Palaeoecol.* 210, 215–233. <https://doi.org/10.1016/j.palaeo.2004.02.042>.
- von Eynatten, H., Barceló-Vidal, C., Pawlowsky-Glahn, V., 2003. Composition and discrimination of sandstones: a statistical evaluation of different analytical methods. *J. Sediment. Res.* 73 (1), 47–57. <https://doi.org/10.1306/070102730047>.
- Farley, K.A., 2002. (U-Th)/He dating: Techniques, calibrations, and applications. In: Porcelli, P.D., Ballentine, C.J., Wieler, R. (Eds.), Noble Gas Geochemistry. Reviews in Mineralogy and Geochemistry 47, pp. 819–843.
- Farley, K.A., Shuster, D.L., Ketcham, R.A., 2011. U and Th zonation in apatite observed by laser ablation ICPMS, and implications for the (U-Th)/He system. *Geochim. Cosmochim. Acta* 75, 4515–4530.
- Faure, M., Lardeaux, J.M., Ledru, P., 2009. A review of the pre-Permian geology of the Variscan French Massif Central. *Compt. Rendus Geosci.* 341, 202–213. <https://doi.org/10.1016/j.crte.2008.12.001>.
- Fernandes, P., Cogné, N., Chew, D.M., Rodrigues, B., Jorge, R.C., Marques, J., Jamal, D., Vasconcelos, L., 2015. The thermal history of the Karoo Moatize-Minjova Basin, Tete Province, Mozambique: an integrated vitrinite reflectance and apatite fission track thermochronology study. *J. Afr. Earth Sci.* 112, 55–72. <https://doi.org/10.1016/j.jafrearsci.2015.09.009>.
- Fleischer, M., Altschuler, Z.S., 1986. The lanthanides and yttrium in minerals of the apatite group - an analysis of the available data. *Neues Jb. Mineral. Monat.* 467–480.
- Fleischer, R.L., Price, P.B., 1964. Techniques for geological dating of minerals by chemical etching of fission fragment tracks. *Geochim. Cosmochim. Acta* 28, 1705–1715.
- Flowers, R.M., Ketcham, R.A., Shuster, D.L., Farley, K.A., 2009. Apatite (U-Th)/He thermochronometry using a radiation damage accumulation and annealing model. *Geochim. Cosmochim. Acta* 73, 2347–2365.
- Foster, G.L., Carter, A., 2007. Insights into the patterns and locations of erosion in the Himalaya—a combined fission-track and in situ Sm–Nd isotopic study of detrital apatite. *Earth Planet. Sci. Lett.* 257, 407–418.
- Frei, D., Liebscher, A., Franz, G., Dulski, P., 2004. Trace element geochemistry of epidote minerals. *Rev. Mineral. Geochem.* 56, 553–605. <https://doi.org/10.2138/gsrmg.56.1553>.
- Gall, Q., Davis, W.J., Lowe, D.G., Dabros, Q., 2017. Diagenetic apatite character and in situ ion microprobe U – Pb age. In: Keeseeville Formation, Potsdam Group, New York State', 797(March), pp. 785–797. <https://doi.org/10.1139/cjes-2016-0195>.
- Gallagher, K., 2012. Transdimensional inverse thermal history modeling for quantitative thermochronology. *J. Geophys. Res. Solid Earth* 117. <https://doi.org/10.1029/2011JB008825>.
- Gallagher, K., Brown, R.W., Johnson, C., 1998. Fission track analysis and its applications to geological problems. *Annu. Rev. Earth Planet. Sci.* 26, 519–572. <https://doi.org/10.1146/annurev.earth.26.1.519>.
- Garzanti, E., 2017. The Maturity Myth in Sedimentology and Provenance Analysis. *J. Sediment. Res.* 87 (4), 353–365. <https://doi.org/10.2110/jsr.2017.17>.
- Garzanti, E., Dinis, P., Vermeesch, P., Andò, S., Hahn, A., Huvi, J., Limonta, M., Padoan, M., Resentini, A., Rittner, M., Vezzoli, G., 2018. Dynamic uplift, recycling, and climate control on the petrology of passive-margin sand (Angola). *Sediment. Geol.* 375, 86–104. <https://doi.org/10.1016/j.sedgeo.2017.12.009>.
- Gawęda, A., Szopa, K., Chew, D., O'Sullivan, G.J., Burda, J., Klötzli, U., Golonka, J., 2018. Variscan post-collisional cooling and uplift of the Tatra Mountains crystalline block constrained by integrated zircon, apatite and titanite LA-(MC)-ICP-MS U-Pb dating and rare earth element analyses. *Chem. Geol.* 484, 191–209. <https://doi.org/10.1016/j.chemgeo.2018.03.012>.
- Gillespie, J., Glorie, S., Khudoley, A., Collins, A.S., 2018. Detrital apatite U-Pb and trace element analysis as a provenance tool: Insights from the Yenisey Ridge (Siberia). *Lithos* 314, 140–155.
- Gleadlow, A.J.W., Duddy, I.R., 1981. A natural long-term track annealing experiment for apatite. *Nuclear Tracks* 5 (1–2), 169–174. [https://doi.org/10.1016/0191-278X\(81\)90039-1](https://doi.org/10.1016/0191-278X(81)90039-1).
- Glorie, S., Alexandrov, I., Nixon, A., Jepson, G., Gillespie, J., Jahn, B.M., 2017. Thermal and exhumation history of Sakhalin Island (Russia) constrained by apatite U-Pb and fission track thermochronology. *J. Asian Earth Sci.* 143, 326–342.
- Glorie, S., Jepson, G., Konopelko, D., Mirkamalov, R., Meeuws, F., Gilbert, S., ... De Grave, J., 2019. Thermochronological and geochemical footprints of post-orogenic fluid alteration recorded in apatite: Implications for mineralisation in the Uzbek Tian Shan. *Gondwana Research* 71 (1–15).
- Goodenough, K.M., Schilling, J., Jonsson, E., Kalvig, P., Charles, N., Tuduri, J., Deady, E.A., Sadeghi, M., Schiellerup, H., Müller, A., Bertrand, G., Arvanitidis, N., Eliopoulos, D.G., Shaw, R.A., Thrane, K., Keulen, N., 2016. Europe's rare earth element resource potential: an overview of REE metallogenetic provinces and their geodynamic setting. *Ore Geol. Rev.* 72, 838–856. <https://doi.org/10.1016/j.oregeorev.2015.09.019>.
- Grapes, R.H., Hoskin, P.W.O., 2004. Epidote group minerals in low-medium pressure metamorphic terranes. *Rev. Mineral. Geochem.* 56, 301–345. <https://doi.org/10.2138/gsrmg.56.1.301>.
- Grimes, C.B., John, B.E., Kelemen, P.B., Mazdab, F.K., Wooden, J.L., Cheadle, M.J., Schwartz, J.J., 2007. Trace element chemistry of zircons from oceanic crust: a method for distinguishing detrital zircon provenance. *Geology* 35 (7), 643–646. <https://doi.org/10.1130/G23603A.1>.
- Harlov, D.E., 2011. Formation of monazite and xenotime inclusions in fluorapatite megacrysts, Glosørhei Granite Pegmatite, Froland, Bamble Sector, southern Norway. *Mineral. Petrol.* 102 (1–4), 77–86. <https://doi.org/10.1007/s00710-011-0166-6>.
- Harlov, D.E., 2015. Apatite: a fingerprint for metasomatic processes. *Elements* 11 (3), 171–176. <https://doi.org/10.2113/gselements.11.3.171>.
- Henderson, A.L., Foster, G.L., Najman, Y., 2010. Testing the application of in situ Sm–Nd isotopic analysis on detrital apatites: a provenance tool for constraining the timing of India-Eurasia collision. *Earth Planet. Sci. Lett.* 297 (1–2), 42–49. <https://doi.org/10.1016/j.epsl.2010.06.001>.
- Henrichs, I.A., O'Sullivan, G.J., Chew, D.M., Mark, C., Babechuk, M.G., McKenna, C., Emo, R., 2018. The trace element and U-Pb systematics of metamorphic apatite.

- Chem. Geol. 483, 218–238. <https://doi.org/10.1016/j.chemgeo.2017.12.031>. Elsevier B.V.
- Henrichs, I.A., Chew, D.M., Sullivan, G.J.O., Mark, C., McKenna, C., Guyett, P., 2019. Trace element (Mn-Sr-Y-Th-REE) and U-Pb isotope systematics of metapelitic apatite during progressive greenschist- to amphibolite-facies Barrovian metamorphism. *Geochim. Geophys. Geosyst.* 20 (8), 4103–4129. <https://doi.org/10.1029/2019GC008359>.
- Hietpas, J., Samson, S., Moecher, D., Schmitt, A.K., 2010. Recovering tectonic events from the sedimentary record: Detrital monazite plays in high fidelity. *Geology* 38 (2), 167–170. <https://doi.org/10.1130/G30265.1>.
- Hoskin, P.W., Ireland, T.R., 2000. Rare earth element chemistry of zircon and its use as a provenance indicator. *Geology* 28 (7), 627–630. [https://doi.org/10.1130/0091-7613\(2000\)28%3C627:RECOZ%3E2.0.CO;2](https://doi.org/10.1130/0091-7613(2000)28%3C627:RECOZ%3E2.0.CO;2).
- Hsieh, P.S., Chen, C.H., Yang, H.J., Lee, C.Y., 2008. Petrogenesis of the Nanling Mountains granites from South China: Constraints from systematic apatite geochemistry and whole-rock geochemical and Sr-Nd isotope compositions. *J. Asian Earth Sci.* 33, 428–451. <https://doi.org/10.1016/j.jseas.2008.02.002>.
- Hubert, J.F., 1962. A zircon-tourmaline-rutile maturity index and the interdependence of the composition of heavy mineral assemblages with the gross composition and texture of sandstones. *J. Sediment. Res.* 32 (3), 440–450. <https://doi.org/10.1306/74D70CE5-2B21-11D7-8648000102C1865D>.
- Hurford, A.J., 2018. An historical perspective on fission-track thermochronology. *Springer Textbooks Earth Sci. Geogr. Environ.* 3–23. [https://doi.org/10.1007/978-3-319-89421-8\\_1](https://doi.org/10.1007/978-3-319-89421-8_1).
- Hurford, A.J., Carter, A., 1991. The role of fission track dating in discrimination of provenance. *Geol. Soc. Lond., Spec. Publ.* 57 (1), 67–78. <https://doi.org/10.1144/GSL.SP.1991.057.01.07>.
- Hurley, P.M., 1954. The helium age method and the distribution and migration of helium in rocks. In: Paul, H. (Ed.), *Nuclear Geology*. John Wiley & Sons, New York, pp. 301–329.
- Ihlen, P.M., Schiellerup, H., Gautneb, H., Skår, Ø., 2014. Characterization of apatite resources in Norway and their REE potential - a review. *Ore Geol. Rev.* 58 (C), 126–147. <https://doi.org/10.1016/j.oregeorev.2013.11.003>.
- Janots, E., Engi, M., Berger, A., Allaz, J., Schwarz, J.O., Spandler, C., 2008. Prograde metamorphic sequence of REE minerals in pelitic rocks of the Central Alps: Implications for allanite-monazite-xenotime phase relations from 250 to 610°C. *J. Metamorph. Geol.* 26, 509–526. <https://doi.org/10.1111/j.1525-1314.2008.00774.x>.
- Joosu, L., Lepland, A., Kirsimäe, K., Romashkin, A.E., Roberts, N.M.W., Martin, A.P., Črni, A.E., 2015. The REE-composition and petrography of apatite in 2Ga Zaonega Formation, Russia: the environmental setting for phosphogenesis. *Chem. Geol.* 395, 88–107. <https://doi.org/10.1016/j.chemgeo.2014.11.013>.
- Joosu, L., Lepland, A., Kreitsmann, T., Üpraus, K., Roberts, N.M.W., Paiste, P., Martin, A.P., Kirsimäe, K., 2016. Petrography and the REE-composition of apatite in the Paleoproterozoic Pilgijärvi Sedimentary Formation, Pechenga Greenstone Belt, Russia. *Geochim. Cosmochim. Acta* 186, 135–153. <https://doi.org/10.1016/j.gca.2016.04.043>.
- Kenny, G.G., O'Sullivan, G.J., Alexander, S., Simms, M.J., Chew, D.M., Kamber, B.S., 2019. On the track of a Scottish impact structure: a detrital zircon and apatite provenance study of the Stac Fada Member and wider Stoer Group, NW Scotland. *Geol. Mag.* 1–14. <https://doi.org/10.1017/S0016756819000220>.
- Ketcham, R.A., 2005. Forward and inverse modeling of low-temperature thermochronometry data. *Rev. Mineral. Geochem.* 58, 275–314.
- King, S.D., 2005. Archean cratons and mantle dynamics. *Earth Planet. Sci. Lett.* 234 (1–2), 1–14. <https://doi.org/10.1016/j.epsl.2005.03.007>.
- Kinny, P.D., Friend, C.R.L., Love, G.J., 2005. Proposal for a terrane-based nomenclature for the Lewisian Gneiss complex of NW Scotland. *J. Geol. Soc.* 162 (1), 175–186. <https://doi.org/10.1144/0016-764903-149>.
- Krenn, E., Harlov, D.E., Finger, F., Wunder, B., 2012. LREE-redistribution among fluorapatite, monazite, and allanite at high pressures and temperatures. *Am. Mineral.* 97, 1881–1890. <https://doi.org/10.2138/am.2012.4005>.
- Kuenen, P.H., 1956. Experimental abrasion of pebbles: 2. Rolling by current. *J. Geol.* 64, 336–368.
- Kuenen, P.H., 1959. Experimental abrasion: 3. Fluvial action on sand. *Am. J. Sci.* 257, 172–190.
- Kuenen, P.H., 1960. Experimental abrasion: 4. Eolian action. *J. Geol.* 68, 427–449.
- Kusebauch, C., John, T., Whitehouse, M.J., Klemme, S., Putnis, A., 2015. Distribution of halogens between fluid and apatite during fluid-mediated replacement processes. *Geochim. Cosmochim. Acta* 170, 225–246. <https://doi.org/10.1016/j.gca.2015.08.023>. Elsevier Ltd.
- Lanari, P., Engi, M., Bern, C., 2017. On Metamorphic Mineral Assemblages. *Rev. Mineral. Geochem.* 83, 55–102. <https://doi.org/10.2138/rmg.2017.83.3>.
- Lawrence, M.G., Kamber, B.S., 2006. The behaviour of the rare earth elements during estuarine mixing-revisited. *Mar. Chem.* 100, 147–161. <https://doi.org/10.1016/j.marchem.2005.11.007>.
- Lê, S., Josse, J., Husson, F., 2008. FactoMineR: an R Package for Multivariate Analysis. *J. Stat. Softw.* 25 (1), 1–18. <https://doi.org/10.1016/j.jenvint.2008.06.007>.
- Li, Y., Klein, C.P.A.T., Zhang, X., De Groot, K., 1993. Relationship between the colour change of hydroxyapatite and the trace element manganese. *Biomaterials* 14 (13), 969–972. [https://doi.org/10.1016/0142-9612\(93\)90187-7](https://doi.org/10.1016/0142-9612(93)90187-7).
- London, D., 1992. Phosphorus in S-type magmas: the P2O5content of feldspars from peraluminous granites, pegmatites, and rhyolites. *Am. Mineral.* 77 (1–2), 126–145.
- Luvizotto, G.L., Zack, T., Triebold, S., Von Eynatten, H., 2009. Rutile occurrence and trace element behavior in medium-grade metasedimentary rocks: example from the Erzgebirge, Germany. *Mineral. Petrol.* 97 (3–4), 233–249. <https://doi.org/10.1007/s00710-009-0092-z>.
- Malusà, M.G., Fitzgerald, P.G., 2019. *Fission-track Thermochronology and its Application to Geology*. Springer International Publishing.
- Malusà, M.G., Polino, R., Zattin, M., Bigazzi, G., Martin, S., Piana, F., 2005. Miocene to present differential exhumation in the Western Alps: Insights from fission track thermochronology. *Tectonics* 24 (3). <https://doi.org/10.1029/2004TC001782>.
- Malusà, M.G., Resentini, A., Garzanti, E., 2016. Hydraulic sorting and mineral fertility bias in detrital geochronology. *Gondwana Res.* 31, 1–19. <https://doi.org/10.1016/j.gr.2015.09.002>.
- Malusa, M.G., Wang, J., Garzanti, E., Liu, Z.C., Villa, I.M., Wittmann, H., 2017. Trace-element and Nd-isotope systematics in detrital apatite of the Po river catchment: Implications for provenance discrimination and the lag-time approach to detrital thermochronology. *Lithos* 290, 48–59. <https://doi.org/10.1016/j.lithos.2017.08.006>.
- Mao, M., Rukhlov, A.S., Rowins, S.M., Spence, J., Coogan, L.A., 2016. Detrital Apatite Trace-Element Compositions: a Robust New Tool for Mineral Exploration. pp. 1. <https://doi.org/10.2113/econgeo.111.5.1187>.
- Mark, C., Cogné, N., Chew, D., 2016. Tracking exhumation and drainage divide migration of the western Alps: a test of the apatite U-Pb thermochronometer as a detrital provenance tool. *GSA Bull.* 1–22. <https://doi.org/10.1130/B31351.1>. In Press(X).
- Matsumoto, T., Honda, M., McDougall, I., Yatsevich, I., O'Reilly, S.Y., 1997. Plume-like neon in a metasomatic apatite from the Australian lithospheric mantle. *Nature* 388 (6638), 162–164. <https://doi.org/10.1038/40606>.
- Mavroforakis, M.E., Theodoridis, S., 2006. A geometric approach to support vector machine (SVM) classification. *IEEE Trans. Neural Netw.* 17 (3), 671–682.
- Mcarthur, J.M., 1985. Francolite geochemistry—compositional controls during formation, diagenesis, metamorphism and weathering. *Geochim. Cosmochim. Acta* 49 (1), 23–35. [https://doi.org/10.1016/0016-7037\(85\)90188-7](https://doi.org/10.1016/0016-7037(85)90188-7).
- McCubbin, F.M., Jolliff, B.L., Nekvasil, H., Carpenter, P.K., Zeigler, R.A., Steele, A., Elardo, S.M., Lindsley, D.H., 2011. Fluorine and chlorine abundances in lunar apatite: Implications for heterogeneous distributions of magmatic volatiles in the lunar interior. *Geochim. Cosmochim. Acta* 75 (17), 5073–5093. <https://doi.org/10.1016/j.gca.2011.06.017>.
- McDonough, W.F., Sun, S., 1995. The composition of the Earth. *Chem. Geol.* 120 (3–4), 223–253. [https://doi.org/10.1016/0009-2541\(94\)00140-4](https://doi.org/10.1016/0009-2541(94)00140-4).
- Meyer, D., Dimitriadou, E., Hornik, K., Weingessel, A., Leisch, F., 2017. e1071: misc functions of the department of statistics, probability theory group (formerly: E1071) TU Wien. R Package Version 1, 6–8.
- Morton, A.C., 1985. A new approach to provenance studies: electron micro probe analysis of detrital garnets from Middle Jurassic sandstones of Northern Sea. *Sedimentology* 32, 553–566. <https://doi.org/10.1111/j.1365-3091.1985.tb00470.x>.
- Morton, A.C., Hallsworth, C.R., 1999. Processes controlling the composition of heavy mineral assemblages in sandstones. *Sediment. Geol.* 124, 3–29. [https://doi.org/10.1016/S0037-0738\(98\)00118-3](https://doi.org/10.1016/S0037-0738(98)00118-3).
- Morton, A., Yaxley, G., 2007. Detrital apatite geochemistry and its application in provenance studies. *Geol. Soc. Am. Spec. Pap.* 420, 319–344. [https://doi.org/10.1130/2006.2420\(19\)](https://doi.org/10.1130/2006.2420(19)).
- Naeser, C.W., 1967. The use of apatite and sphene for fission track age determinations. *Geol. Soc. Am. Bull.* 78, 1523–1526.
- Nechaev, V.P., Ispahring, W.C., 1993. Heavy-mineral assemblages of continental margins as indicators of plate-tectonic environments. *J. Sediment. Petrol.* 63 (6), 1110–1117. <https://doi.org/10.1036/D4267CB7-2B26-11D7-8648000102C1865D>.
- Nishizawa, M., Takahata, N., Terada, K., Komiya, T., Ueno, Y., Sano, Y., 2005. Rare-earth element, lead, carbon, and nitrogen geochemistry of apatite-bearing metasediments from the similar to 3.8 Ga Isua supracrustal belt, West Greenland. *Int. Geol. Rev.* 47 (9), 952–970. <https://doi.org/10.2747/0020-6814.47.9.952>.
- Nutman, A.P., 2007. Apatite recrystallisation during prograde metamorphism, Cooma, Southeast Australia: implications for using an apatite – graphite association as a biotracer in ancient metasedimentary rocks. *Aust. J. Earth Sci.* 54, 1023–1032. <https://doi.org/10.1080/08120090701488321>.
- O'Reilly, S.Y., Griffin, W.L., 2000. Apatite in the mantle: Implications for metasomatic processes and high heat production in Phanerozoic mantle. *Lithos* 53 (3–4), 217–232. [https://doi.org/10.1016/S0024-4937\(00\)00026-8](https://doi.org/10.1016/S0024-4937(00)00026-8).
- O'Sullivan, G.J., Chew, D.M., Samson, S.D., 2016. Detecting magma poor orogens in the detrital record. *Geology* 44 (10), 871–874. <https://doi.org/10.1130/G38245.1>.
- O'Sullivan, G.J., Chew, D.M., Morton, A.C., Mark, C., Henrichs, I.A., 2018. An integrated apatite geochronology and geochemistry tool for sedimentary provenance analysis. *Geochim. Geophys. Geosyst.* 1309–1326. <https://doi.org/10.1002/2017GC007343>.
- Oosthuizen, E.J., Burger, A.J., 1973. The suitability of apatite as an age indicator by the uranium-lead isotope method. *Earth Planet. Sci. Lett.* 18 (1), 29–36. [https://doi.org/10.1016/0012-821X\(73\)90030-7](https://doi.org/10.1016/0012-821X(73)90030-7).
- Owen, M.R., 1987. Hafnium content of detrital zircons, a new tool for provenance study. *J. Sediment. Petrol.* 57, 824–830. <https://doi.org/10.1306/212F8C74-2B24-11D7-8648000102C1865D>.
- Parnell, J., Mark, D., Fallick, A.E., Boyce, A., Thackrey, S., 2011. The age of the mesoproterozoic stoer group sedimentary and impact deposits, NW Scotland. *J. Geol. Soc.* 168 (2), 349–358. <https://doi.org/10.1144/0016-76492010-099>.
- Paton, C., Hellstrom, J., Paul, B., Woodhead, J., Hergt, J., 2011. Iolite: Freeware for the visualisation and processing of mass spectrometric data. *J. Anal. At. Spectrom.* 26 (12), 2508. <https://doi.org/10.1039/c1ja0172b>.
- Picard, M.D., McBride, E.F., Arribas, J., Johnsson, M.J., Critelli, S., 2007. Comparison of river and beach sand composition with source rocks, Dolomite Alps drainage basins, northeastern Italy. *Geol. Soc. Am. Spec. Pap.* 420, 1–12. [https://doi.org/10.1130/2007.2420\(01\)](https://doi.org/10.1130/2007.2420(01)).
- Piccoli, P.M., Candela, P.A., 2002. Apatite in Igneous Systems. *Rev. Mineral. Geochem.* 48, 255–292. <https://doi.org/10.2138/rmg.2002.48.6>.
- Prowatke, S., Klemme, S., 2006. Trace element partitioning between apatite and silicate

- melts. *Geochim. Cosmochim. Acta* 70 (17), 4513–4527. <https://doi.org/10.1016/j.gca.2006.06.162>.
- Ricketts, J.W., Kelley, S.A., Karlstrom, K.E., Schmandt, B., Donahue, M.S., van Wijk, J., 2016. Synchronous opening of the Rio Grande rift along its entire length at 25–10 Ma supported by apatite (U-Th)/he and fission-track thermochronology, and evaluation of possible driving mechanisms. *GSA Bull.* 128 (3–4), 397–424.
- Ronsbo, J.G., 1989. Coupled substitutions involving REEs and Na and Si in apatites in alkaline rocks from the Ilímaussaq intrusion, South Greenland, and the petrological implications. *Am. Mineral.* 74 (7–8), 896–901.
- Roycroft, P.D., Cuypers, M., 2015. The etymology of the mineral name ‘Apatite’: a clarification. *Irish J. Earth Sci.* 33, 71–75. <https://doi.org/10.3318/ijes.2015.33.71>.
- Russell, R.D., 1937. Mineral composition of Mississippi River sands. *Geol. Soc. Am. Bull.* 48, 1307–1348.
- Ruttenberg, K.C., Berner, R.A., 1993. Authigenic apatite formation and burial in sediments from non-upwelling, continental margin environments. *Geochim. Cosmochim. Acta* 57 (5), 991–1007. [https://doi.org/10.1016/0016-7037\(93\)90035-U](https://doi.org/10.1016/0016-7037(93)90035-U).
- Samson, S., Matthews, S., Mitchell, C., Goldman, D., 1995. Tephrochronology of highly altered ash beds: the use of trace element and Sr isotope geochemistry of apatite phenocrysts to correlate K-bentonites. *Geochim. Cosmochim. Acta* 59 (12), 2527–2536. [https://doi.org/10.1016/0016-7037\(95\)00147-6](https://doi.org/10.1016/0016-7037(95)00147-6).
- Schneider, S., Hammerschmidt, K., Rosenberg, C.L., Gerdes, A., Frei, D., Bertrand, A., 2015. U-Pb ages of apatite in the western Tauern Window (Eastern Alps): Tracing the onset of collision-related exhumation in the European plate. *Earth Planet. Sci. Lett.* 418, 53–65. <https://doi.org/10.1016/j.epsl.2015.02.020>. Elsevier B.V.
- Sell, B.K., Samson, S.D., 2011. A tephrochronologic method based on apatite trace-element chemistry. *Quat. Res.* 76 (1), 157–166. <https://doi.org/10.1016/j.yqres.2011.03.007>. Cambridge University Press.
- Sell, B.K., Samson, S.D., Mitchell, C.E., McLaughlin, P.I., Koenig, A.E., Leslie, S.A., 2015. Stratigraphic correlations using trace elements in apatite from late Ordovician (Sandbian-Katian) K-bentonites of eastern North America the early late Ordovician sedimentary. *Geol. Soc. Am. Bull.* 9, 1–16. <https://doi.org/10.1130/B31194.1>.
- Sha, L.-K., Chappell, B.W., 1999. Apatite chemical composition, determined by electron microprobe and laser-ablation inductively coupled plasma mass spectrometry, as a probe into granite petrogenesis. *Geochim. Cosmochim. Acta* 63 (22), 3861–3881. [https://doi.org/10.1016/S0016-7037\(99\)00210-0](https://doi.org/10.1016/S0016-7037(99)00210-0).
- Shields, G., Stille, P., 2001. Diagenetic constraints on the use of cerium anomalies as palaeoseawater redox proxies: an isotopic and REE study of Cambrian phosphorites. *Chem. Geol.* 175 (1–2), 29–48. [https://doi.org/10.1016/S0009-2541\(00\)00362-4](https://doi.org/10.1016/S0009-2541(00)00362-4).
- Simms, M.J., 2015. The Stac Fada impact ejecta deposit and the Lairg Gravity Low: evidence for a buried Precambrian impact crater in Scotland? *Proc. Geol. Assoc.* 126 (6), 742–761. <https://doi.org/10.1016/j.pgeola.2015.08.010>. The Geologists’ Association.
- Spear, F.S., Pyle, J.M., 2002. Apatite, Monazite, and Xenotime in Metamorphic Rocks. *Rev. Mineral. Geochem.* 48, 293–335. <https://doi.org/10.2138/rmg.2002.48.7>.
- Spencer, C.J., Kirkland, C.L., Taylor, R.J.M., 2016. Strategies towards statistically robust interpretations of in situ U-Pb zircon geochronology. *Geosci. Front.* 7 (4), 581–589. <https://doi.org/10.1016/j.gsf.2015.11.006>. Elsevier Ltd.
- Stewart, A.D., 2002. The later Proterozoic Torridonian rocks of Scotland: their sedimentology, geochemistry and origin. *Geol. Soc. Lond. Mem.* 24 (130), 5–21.
- Stock, G.M., Ehlers, T.A., Farley, K.A., 2006. Where does sediment come from? Quantifying catchment erosion with detrital apatite (U-Th)/ he thermochronometry. *Geology* 34 (9), 725–728. <https://doi.org/10.1130/G22592.1>.
- Stockli, D.F., Farley, K.A., Dumitru, T.A., 2000. Calibration of the (U-Th)/he thermochronometer on an exhumed fault block, White Mountains, California. *Geology* 28 (2000), 983–986.
- Strutt, R.J., 1908. On the accumulation of helium in geological time. In: Proceedings of the Royal Society of London. Series A, Containing Papers of a Mathematical and Physical Character. 81(547). pp. 272–277. <https://doi.org/10.1098/rspa.1908.0079>.
- Tang, M., Wang, X.L., Xu, X.S., Zhu, C., Cheng, T., Yu, Y., 2012. Neoproterozoic subducted materials in the generation of Mesozoic Luzong volcanic rocks: evidence from apatite geochemistry and Hf-Nd isotopic decoupling. *Gondwana Res.* 21 (1), 266–280. <https://doi.org/10.1016/j.gr.2011.05.009>. International Association for Gondwana Research.
- Thomson, S.N., Gehrels, G.E., Ruiz, J., Buchwaldt, R., 2012. Routine low-damage apatite U-Pb dating using laser ablation-multicollector-ICPMS. *Geochem. Geophys. Geosyst.* 13 (1), 1–23. <https://doi.org/10.1029/2011GC003928>.
- Tollari, N., Barnes, S.J., Cox, R.A., Nabil, H., 2008. Trace element concentrations in apatites from the Sept-Îles Intrusive Suite, Canada - Implications for the genesis of nelsonites. *Chem. Geol.* 252 (3–4), 180–190. <https://doi.org/10.1016/j.chemgeo.2008.02.016>.
- Tyrrell, S., Haughton, P.D.W., Daly, J.S., 2007. Drainage reorganization during breakup of Pangea revealed by in-situ Pb isotopic analysis of detrital K-feldspar. *Geology* 35, 971–974. <https://doi.org/10.1130/G4123A.1>.
- Vapnik, V., 2013. *The Nature of Statistical Learning Theory*. Springer Science & Business Media.
- Vermeesch, P., Avigad, D., McWilliams, M.O., 2009. 500 m.y. of thermal history elucidated by multi-method detrital thermochronology of North Gondwana Cambrian sandstone (Eilat area, Israel). *Bull. Geol. Soc. Am.* 121 (7–8), 1204–1216. <https://doi.org/10.1130/B26473.1>.
- Wagner, G.A., 1968. Fission track dating of apatites. *Earth Planet. Sci. Lett.* 4 (5), 411–415. [https://doi.org/10.1016/0012-821X\(68\)90072-1](https://doi.org/10.1016/0012-821X(68)90072-1).
- Wallis, D., Carter, A., Phillips, R.J., Parsons, A.J., Searle, M.P., 2016. Spatial variation in exhumation rates across Ladakh and the Karakoram: New apatite fission track data from the Eastern Karakoram, NW India. *Tectonics* 35 (3), 704–721. <https://doi.org/10.1002/2015TC003943>.
- Webb, W.V.A., Briggs, L.I., 1966. The use of principal component analysis to screen mineralogical data. *J. Geol.* 74, 716–720.
- Weltje, G.J., 2012. Quantitative models of sediment generation and provenance: state of the art and future developments. *Sediment. Geol.* 280, 4–20.
- Whittaker, E.J.W., Muntus, R., 1970. Ionic radii for use in geochemistry. *Geochim. Cosmochim. Acta* 34 (9), 945–956.
- Wickham, H., 2011. *ggplot2*. 3(2). Wiley Interdisciplinary Reviews: Computational Statistics, pp. 180–185.
- Wolf, R.A., Farley, K.A., Silver, L.T., 1996. Helium diffusion and low-temperature thermochronometry of apatite. *Geochim. Cosmochim. Acta* 60 (21), 4231–4240.
- Zattin, M., Andreucci, B., Thomson, S.N., Reiners, P.W., Talarico, F.M., 2012. New constraints on the provenance of the ANDRILL AND-2A succession (western Ross Sea, Antarctica) from apatite triple dating. *Geochem. Geophys. Geosyst.* 13 (10). <https://doi.org/10.1029/2012GC004357>.
- Zeitler, P.K., Herczeg, A.L., McDougall, I., Honda, M., 1987. U-Th-He dating of apatite: a potential thermochronometer. *Geochim. Cosmochim. Acta* 51 (10), 2865–2868. [https://doi.org/10.1016/0016-7037\(87\)90164-5](https://doi.org/10.1016/0016-7037(87)90164-5).
- Zirner, A.L.K., Marks, M.A.W., Wenzel, T., Jacob, D.E., Markl, G., 2015. Rare earth elements in apatite as a monitor of magmatic and metasomatic processes: The Ilímaussaq complex, South Greenland. *Lithos* 228–229, 12–22. <https://doi.org/10.1016/j.lithos.2015.04.013>. Elsevier B.V.